

We are IntechOpen, the world's leading publisher of Open Access books Built by scientists, for scientists

6,900

Open access books available

186,000

International authors and editors

200M

Downloads

Our authors are among the

154

Countries delivered to

TOP 1%

most cited scientists

12.2%

Contributors from top 500 universities



WEB OF SCIENCE™

Selection of our books indexed in the Book Citation Index
in Web of Science™ Core Collection (BKCI)

Interested in publishing with us?
Contact book.department@intechopen.com

Numbers displayed above are based on latest data collected.
For more information visit www.intechopen.com



The Role of the Antigen GAD 65 in Diabetes Mellitus Type 1: A Molecular Analysis

Marco Wiltgen and Gernot P. Tilz

Additional information is available at the end of the chapter

<http://dx.doi.org/10.5772/48329>

1. Introduction

Diabetes mellitus patients have a high blood sugar (glucose) level resulting either from the body's failure to produce enough insulin (Diabetes Mellitus Type 1) or because body cells do not properly respond to the produced insulin (Diabetes Mellitus Type 2) [1,2]. During the digestion, carbohydrates, contained in food, are converted within a few hours to glucose. Insulin is a hormone produced in the pancreas that enables body cells (primarily muscle and fat cells) to absorb glucose which is in turn transformed into energy needed for daily life [3,4]. The insulin production is triggered by the increase of the glucose concentration in blood (Figure 1).

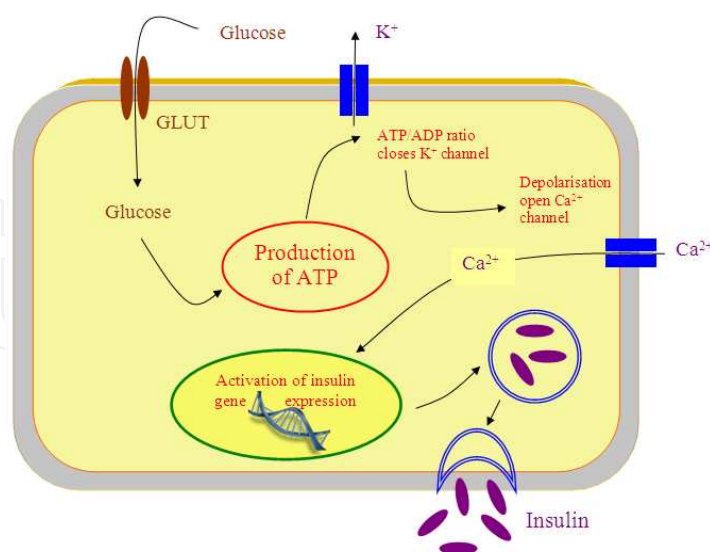


Figure 1. By the decomposition of glucose, ATP is produced in the beta cells. The increase of the ATP concentration closes the K⁺ channel, leading to a depolarisation which in consequence opens the Ca²⁺ channel. Ca²⁺ activates the insulin gene expression via the Calcium Responsive Element Binding Protein (CREB). By exocytosis, the produced insulin is set free in the blood.

The regulatory function of insulin results in an instantly higher reception of glucose after the meals (Figure 2). Normally, insulin regulates the uptake of glucose from the blood during the course of a day (Figure 3). The inability of the body cells to absorb the glucose results in an accumulation (casual plasma glucose: 11.1 mmol/L) in the blood (hyperglycemia), leading to various potential medical complications and commonly leads to coma [5,6]. If the glucose concentration in the blood exceeds a certain amount it is discharged via the urine. Serious long-term complications of diabetes mellitus include cardiovascular disease, chronic renal failure and retinal damage [7-10]. Diabetes mellitus is currently a worldwide epidemic disease, sometimes referred as epidemic disease of the 21-th century [11,12]. Therefore an early diagnosis is desirable, enabling prevention at begin of this autoimmune disease.

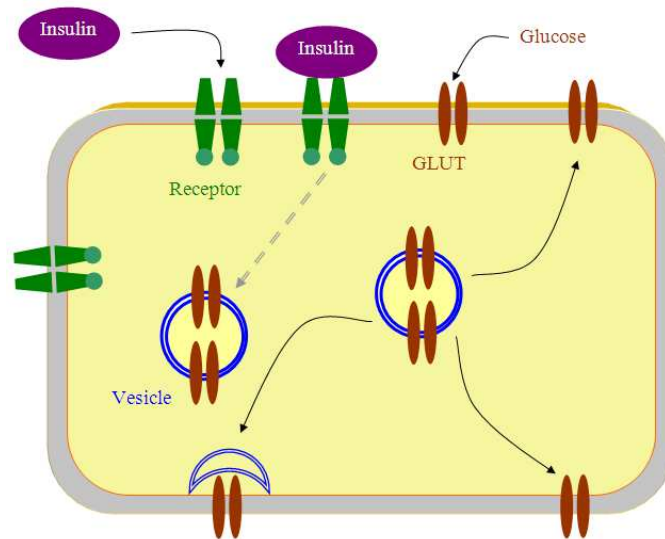


Figure 2. The hormone insulin induces the reception of glucose into the cells by a member of the transport protein GLUT. The binding of insulin at receptors, located at the cell surface, initiates the fusion of intracellular vesicles, containing GLUT, with the cell membrane. This increases instantly the number of the GLUT molecules at the cell surface, resulting in a higher reception of glucose.

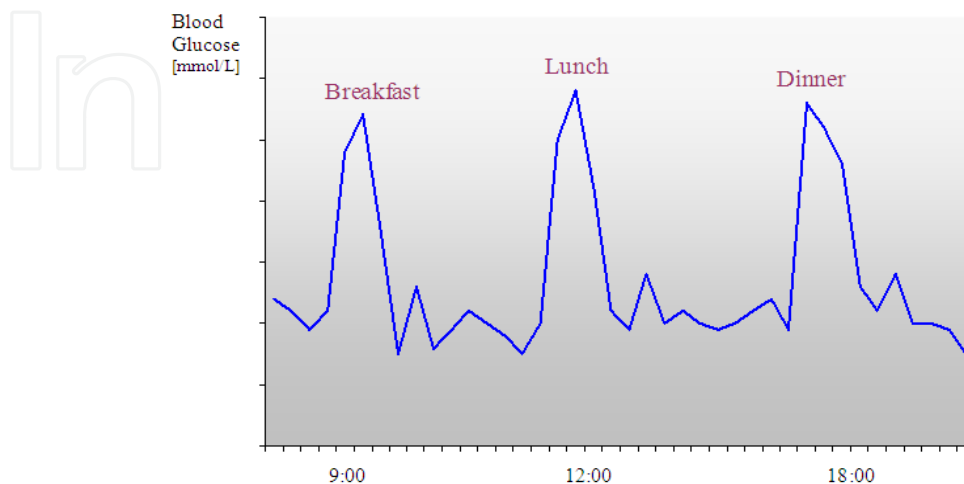


Figure 3. Qualitative view of the fluctuation of the blood sugar concentration in humans during the course of a day with 3 meals.

Diabetes mellitus type 1 result from the inability of the body to produce endogenous insulin; in consequence the patient must inject the required insulin, either manually or automatically via an insulin pump [13-14]. This is a major burden, because the insulin therapy, management and monitoring of diabetes is necessary for the rest of patient's life [15]. Goal of the insulin therapy is not the healing of the patient, but the replacement of the lack of endogenous insulin. Diabetes mellitus type 1 includes childhood-onset diabetes, juvenile diabetes, and insulin-dependent diabetes mellitus (IDDM) [16]. The type 1 diabetes causes approximately 10% of diabetes mellitus cases worldwide and represents a majority of diabetes in children [17]. Recent publications show that a doubling of diabetes mellitus type 1 in childhood (younger than 5 years) is expected by 2020, and in the juvenile age (younger than 15 years), the disease will rise by 70% [18]. Diabetes mellitus type 1 is characterized by a loss of the insulin-producing beta cells of the islets of Langerhans in the pancreas [19] (Figure 4). The majority of diabetes mellitus type 1 cases is of an immune-mediated nature, where the loss of beta cell results from a T-cell mediated autoimmune attack (antibodies: GADA, ICA, IA-2, IAA) [20]. After 80-90% of the beta cells are destroyed, the diabetes mellitus type 1 manifests. Therefore, at the start of the disease there is still a remaining insulin production. Mostly, at the onset of the disease, the affected people are otherwise healthy and of normal weight. In the early stages, the sensitivity and responsiveness to insulin are usually normal. The symptoms of diabetes mellitus are frequent urination (polyuria), increased thirst (polydipsia) and increased hunger (polyphagia) [21]. (Originally, the main symptom was excessive sweet urine, known as glycosuria). Diabetes mellitus type 1 may also cause a rapid weight loss and irreducible mental fatigue.

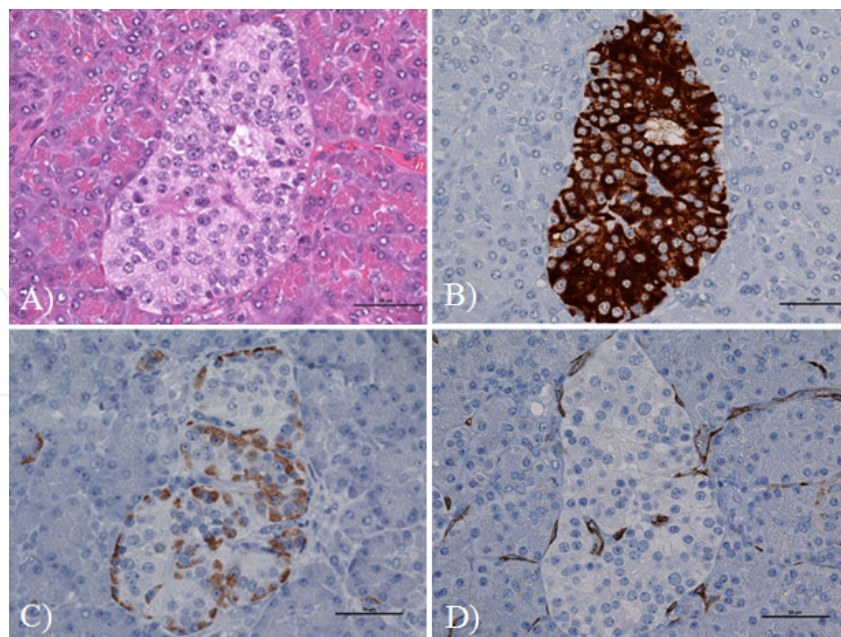
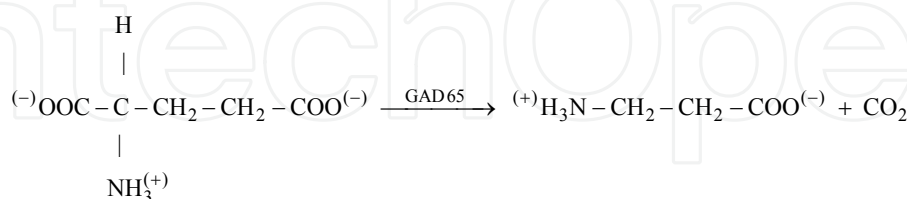


Figure 4. A) The cells of the islets of Langerhans (large object in the middle) in the pancreas produce insulin, which is secreted directly into the blood flow. Immune histochemistry with antibodies against: B) insulin (representation of the beta cells), C) glucagon (alpha cells), D) CD34 (capillaries). Picture provided by the Institute for Pathology of the Medical University of Graz (C. Lackner).

Whereas diabetes type 2 is mainly caused by lifestyle factors (such as smoking, elevated cholesterol levels, obesity, high blood pressure) and inheritance, diabetes type 1 seems to be only partly inherited, by mutations of the major histocompatibility complex (MHC) at chromosome 6, and requires an environmental trigger (possibly due to an infection). Certain infections, with some evidence pointing at Coxsackie B4 virus, rubella virus and others are considered risk factors [22-25]. Various nutritional risk factors, such as; the consumption of cow milk; early exposure to the protein gluten existing in some grass-related grains, notably wheat, rye, and barley, have been studied [26-28]. Bafilomycine, which is produced at decayed places in potatoes by streptomycetes, leads to a glucose intolerance and damage to the islets of Langerhans in the pancreas. To explain the reaction of the autoimmune mechanism, it is assumed that certain bacteria and virus appears (from the point of view of the antibodies) similar to the cells of the pancreas (more precisely to a protein at the cell surface) and therefore the body destroys not only the infiltrated bacteria and virus but also attacks its own cells. Some sub structures of the antigens are similar to insulin and therefore trigger the autoimmune attack to the pancreas. Because insulinitis, an inflammation of the islets of Langerhans of the pancreas, is considered to be a preliminary stage of diabetes mellitus type 1, an diminishing of the inflammation processes is considered to be a possible immune-therapeutically measure for the prevention of diabetes. The inflammation begins mostly in the childhood or at juvenile age.

For diabetes mellitus type 1, islet cell auto-antibodies (ICA) could be detected in 80% of the cases [29]. Other auto-antibodies are insulin-antibodies (IAA) and tyrosinphosphatase-antibodies (IA-2) [30]. The glutamic acid decarboxylase antibody (GADA) specifically attacks the enzyme glutamic acid decarboxylase (GAD 65) in the beta cells [31-34]. (65 refers to the molecular mass of 65kD). This antibody is an indication for diabetes type 1, although it is present in only 50-70% of the cases at the onset of the disease and at later stages successively more rarely. The GAD 65 gene is expressed in brain cells and in the beta cells of the pancreas. Inside the beta cells, the enzyme GAD 65 (EC 4.1.1.15) catalyzes the irreversible alpha-decarboxylation of L-glutamate into gamma-aminobutyrate (GABA) and carbon dioxide. (GABA is used as a neurotransmitter in the brain).



GAD uses pyridoxal-phosphate (PLP) as a cofactor. GAD 65 is a homo dimer (it consists of two identical chains), characterized by successively 4 stranded β -sheets and 7 stranded β -sheets (Figure 5). The enzyme that can provoke an autoimmune reaction against the beta cells of the pancreas progressing to type 1 diabetes mellitus [35]. The GAD 65 antigen was considered to be strictly located intra-cytoplasmatic in the beta cells of the pancreas. But this hypothesis can not explain the procedure of immunization and therefore the occurrence of GAD 65 antibodies in the blood.

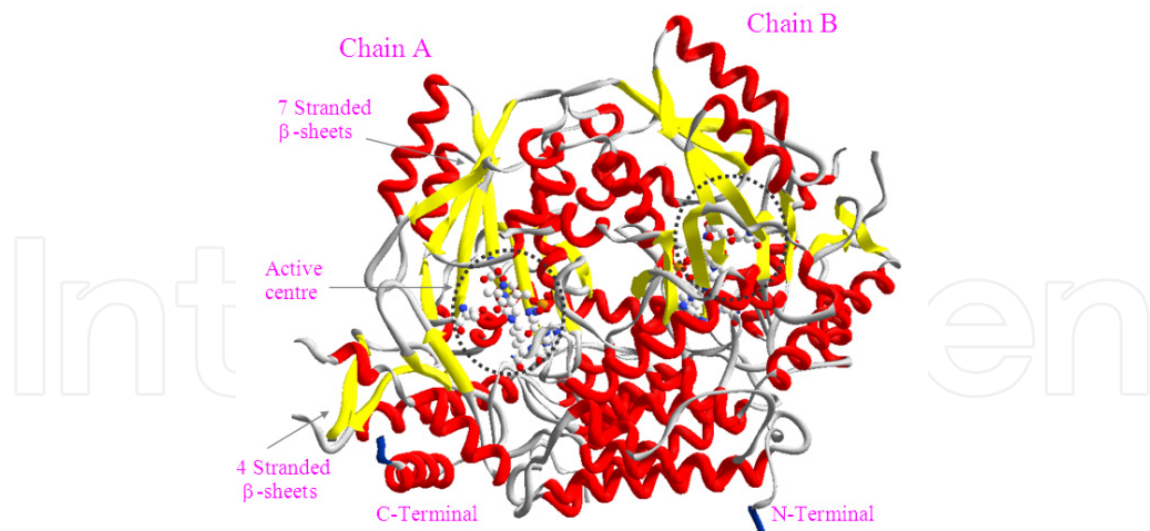


Figure 5. The enzyme GAD 65 is a dimer. Each chain contains 4 stranded β -sheets (yellow) surrounded by three α -helices (red) and 7 stranded β -sheets surrounded by eight α -helices. Every chain has an own active centre.

To understand the procedure and development of immunization, it was proposed that in an initial step the immune system is primed by the accessibility to GAD 65 [36,37]. The assumption is that the enzyme has to be in the human serum and should be found in higher concentrations before the onset of the disease. The proof and quantitative evaluation of GAD 65 in the human blood is done with the Fluorescence Correlation Spectroscopy (FCS), the Enzyme-Linked Immunosorbent Assay (ELISA) and the Surface enhanced laser desorption ionisation – time of flight (SELDI-TOF) system.

To illustrate the mechanism of autoimmunization, the visualization of the GAD 65 tertiary structure, together with its antigenic determinants and the associated electrostatic field, is essential. The 3-D molecular surface, derived from space filling models, visualizes the fitting of the GAD 65 epitopes to the paratopes of the antibodies and quantitative values for the GAD 65 antigenic properties are obtained by dual models. The electrostatic potential and details of the electronic structure of the GAD 65 epitopes are calculated by quantum theoretical methods. Readers, not interested in theoretical and mathematical details, can omit the corresponding chapters as the figures enable a pictorial understanding of the principles.

2. Measurement of GAD 65 in human sera

The GAD 65 molecules are detected by the binding with their unique and specific antibodies, which enables it to pick out the GAD 65 molecules in a mixture of different molecules (Figure 6). All detection methods, used in this work, are based on this principle. The monoclonal antibodies Z1 and Z2, provided by Phadia, Sweden-Diagnostics, Freiburg/Breisgau, Germany, were used for the detection of GAD 65 in all the assays. Antibody Z1 and antibody Z2 are reacting with different epitopes of the GAD 65 molecule.

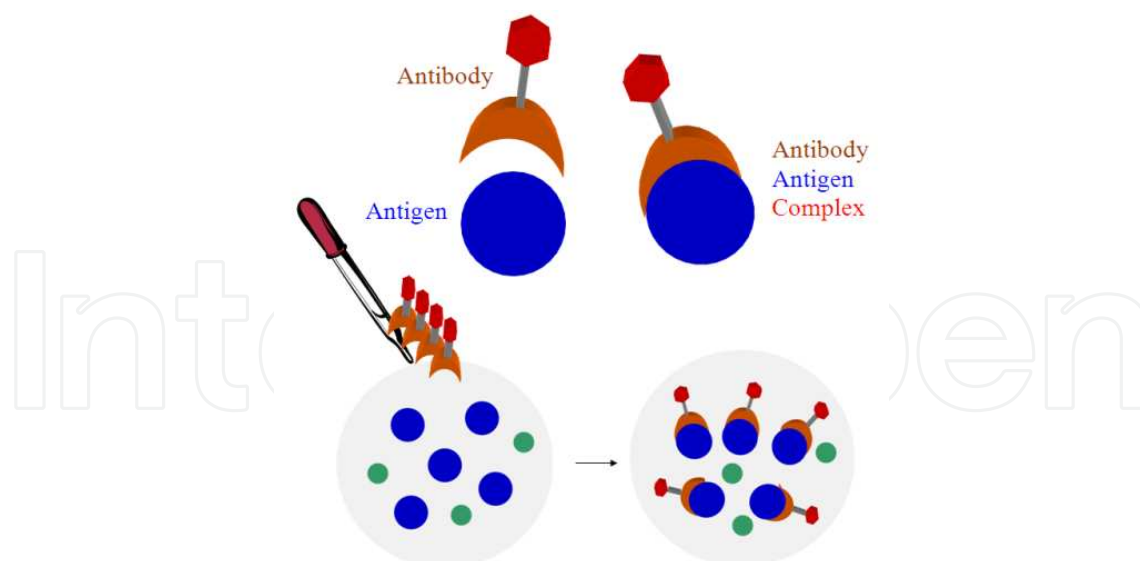


Figure 6. Antigens, like GAD 65, are detected by specific capturing with their corresponding antibodies. This enables it to pick up the antigen GAD 65 from a mixture of molecules.

Because very small concentrations of GAD 65 circulating in the human sera were expected, the ultra-sensitive fluorescence correlation spectroscopy (FCS) was used, at the beginning, for the search of free circulating GAD 65.

2.1. Fluorescence Correlation Spectroscopy (FCS)

FCS is a very sensitive analytical tool which enables the observation of a small number of molecules (up to picomolar concentrations) in a small volume element. By the FCS, the information about the molecules in the volume element is gained by evaluation of fluorescence fluctuations. FCS was developed by D. Magde, E. Elson, and W.W. Webb in 1972 [38]. The development of sensitive detectors such as avalanche photodiodes makes it possible to detect fluorescence signals coming from individual molecules in highly diluted samples. Improvements in the measurement techniques, notably by the introduction of confocal microscopy, enable a more precise separation of the measurement volume from the background. This improved the signal-to-noise ratio and allowed single molecule detection. In the 1990's began the practical application of FCS in molecular biology, ranging from the study of molecular dynamics, the determination of the size of proteins and the antigen-antibody coupling to the study of biochemical pathways in living cells.

2.1.1. Configuration and principle

With the FCS method, the GAD 65 molecules and their interaction with the corresponding monoclonal antibodies are measured by determining their diffusion times in a tiny volume element [39-43]. For this purpose the antibody molecules are labelled with fluorescent markers and excited by laser light. Because fluorochromes come in a variety of colours and can be specifically bound to particular molecules it is possible to study the behavior of individual molecules.

The FCS setup consists of a laser, an inverted microscope, a beam splitter (dichroic mirror), several optical units, a spectrometer with photo diode and an evaluation unit (Figure 7). The laser beam is directed by the beam splitter through the inverted microscope and focussed into a small focal volume of the sample. The labelled molecules in the sample are excited and emit fluorescence light. The emitted fluorescence light passes through the inverted microscope and the beam splitter. The beam splitter separates the excitation light from the emitted fluorescence light by transmitting the fluorescence light to the spectrometer and reflecting the excitation light back to the microscope. The transmitted fluorescence light then passes through a pinhole which blocks scattered excitation light and fluorescence light from outside the focal spot. The intensity of the filtered light is measured by avalanche photo diodes. The evaluation of the FCS measurement results is based on auto-correlation and cross-correlation analysis of the fluorescence fluctuations.

The optical unit of the FCS set up used in this study consists of a ConfoCor 2 (Zeiss) spectrometer and a confocal Zeiss Axiovert 100 microscope. An Argon ion-laser (458, 488, 514 nm) and 2 Helium neon lasers (543, 633 nm) are used for the excitation of the fluorescent molecules. The laser-light is concentrated by a C-Apochromat objective ($\times 40/1.2$ W corr.) on small spots (diameter: $0.5 \mu\text{m}$) in the sample solution. The GAD antibodies, were pipetted into a borosilicate chamber (Nalge Nunc, Lab Tek. chambered cover glass, German borosilicate cover glass, 8 chamber version), located on top of the inverted microscope.

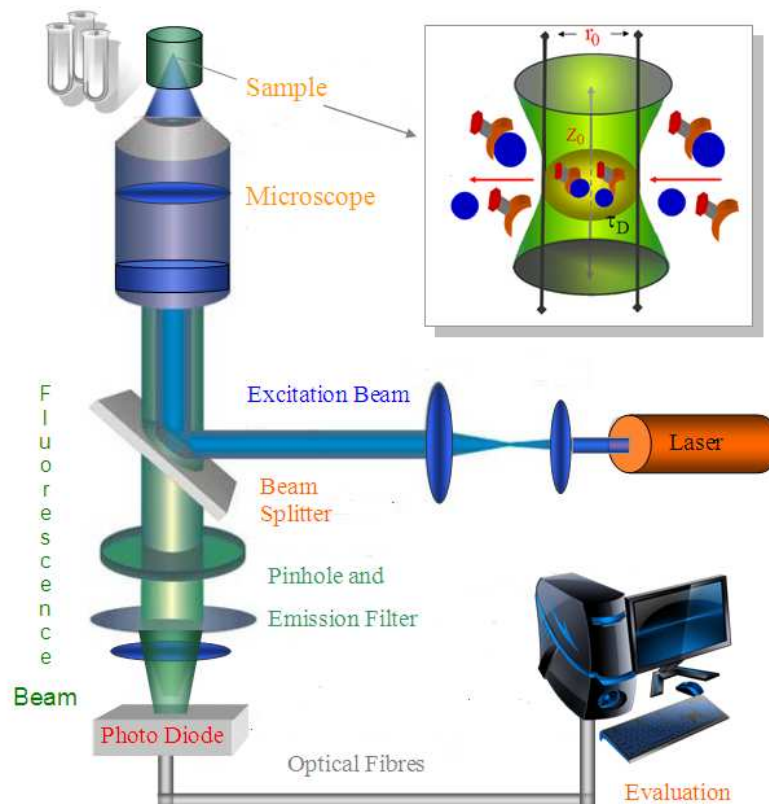


Figure 7. Set up and principle of the Fluorescence Correlation Spectroscopy (the radius r_0 is approximately $0.5 \mu\text{m}$).

2.1.2. Evaluation of the fluorescence signal

The fluorescence intensity is fluctuating due to the Brownian motion of the molecules through the focal volume element, defined by the optical system, whereby the concentration of the particles $c(r, t)$ is randomly fluctuating around the average concentration $\langle C \rangle$:

$$\delta c(r, t) = c(r, t) - \langle C \rangle \quad (1)$$

The analysis gives the average number of fluorescent particles and average diffusion time, when the particle is passing through the volume. Since the relative fluctuations become smaller with increasing numbers of measured molecules, it is important to minimize the number of molecules in the focal volume. Changes in the diffusion times yield conclusions about the binding of GAD 65 to the corresponding antibody. The diffusion time of the labelled molecules depends on their size, therefore antigen-antibody compounds, which are bigger, show a slower diffusion time than the separated individual molecules. Modifications of the diffusion times give the required information on existence and concentration of GAD 65 in the specimens.

The fluorescence intensity fluctuations are recorded over time and quantified by temporally auto-correlation. From the auto-correlation and cross-correlation analysis of the fluorescence signal, results the characteristic diffusion times of the molecules. By the auto-correlation analysis, the measured fluorescence signal is compared with itself at some later time. The detected fluorescence signal intensity $I(t)$, at time step t , fluctuates around the mean intensity value $\langle I(t) \rangle$. The fluctuations of the emitted fluorescence signal are defined as the deviations from the temporal average of the signal:

$$\delta I(t) = I(t) - \langle I(t) \rangle \quad (2)$$

Whereby the mean intensity over the time period T is defined by:

$$\langle I(t) \rangle = \frac{1}{T} \int_0^T I(t') dt' \quad (3)$$

The auto-correlation function $G(\tau)$ combines the average fluctuation of the molecule at time step t with its fluctuation shifted by time τ (correlation time). The normalized auto-correlation function is defined as:

$$G(\tau) = \frac{\langle \delta I(t) \cdot \delta I(t + \tau) \rangle}{\langle I(t) \rangle^2} \quad (4)$$

The auto-correlation amplitude $G(0)$ is the normalized variance of the fluctuating fluorescence signal. If all fluctuations arise from changes in the local concentration of the molecules within the volume element of the focal spot, the variations in the fluorescence intensity can be written as:

$$\delta I(t) = \int_V W(r) \delta c(r, t) dV \quad (5)$$

The term $\delta(c(r, t))$ determines the dynamics of the molecules: $\delta c(r, t)$ describes the fluctuations in the local molecule concentration at time t . The function $W(r)$ describes the spatial distribution of the emitted fluorescence light. Substituting the expression for the intensity fluctuations into the auto-correlation function yields:

$$G(\tau) = \frac{\iint W(r)W(r') \langle \delta(c(r, t)) \delta(c(r', t + \tau)) \rangle dV dV'}{\left(\int W(r) \delta(c(r, t)) dV \right)^2} \quad (6)$$

The auto-correlation function $G(\tau)$ is characterized by the correlation time τ and the correlation amplitude $G(0)$. Every process, producing fluctuations in the fluorescence intensity, has a characteristic correlation time. The FCS output by itself only represents a time spectrum. Interpretations on physical phenomena have to be extracted from the auto-correlation function by developing appropriate physical models. The parameters of interest are found after fitting the auto-correlation curve to modeled functional forms.

2.1.3. Model of free diffusion

If the model of free diffusion is used, the fluctuation signal is characterized by the diffusion time (in-out motion of the molecules in the volume element) and the average number of molecules in the volume element (Figure 8). The spatial and timely distribution of the molecule concentration in the model of free diffusion is given by the differential equation:

$$\frac{\partial}{\partial t} c(r, t) = D \left(\frac{\partial^2}{\partial x^2} + \frac{\partial^2}{\partial y^2} + \frac{\partial^2}{\partial z^2} \right) c(r, t) \quad (7)$$

This implies that the molecules are freely diffusing in three dimensions with the diffusion coefficient D . The larger the mass of the molecule, the larger is the diffusion time and in consequence the fluctuation is getting slower (Figure 8). The spatial distribution of the emitted fluorescence light $W(r)$ is approximated by a three dimensional Gaussian distribution:

$$W(r) = \exp\left(-2 \frac{x^2 + y^2}{r_0^2}\right) \exp\left(-\frac{z^2}{z_0^2}\right) \quad (8)$$

With:

$$r_0 = \sqrt{x_0^2 + y_0^2} \quad (9)$$

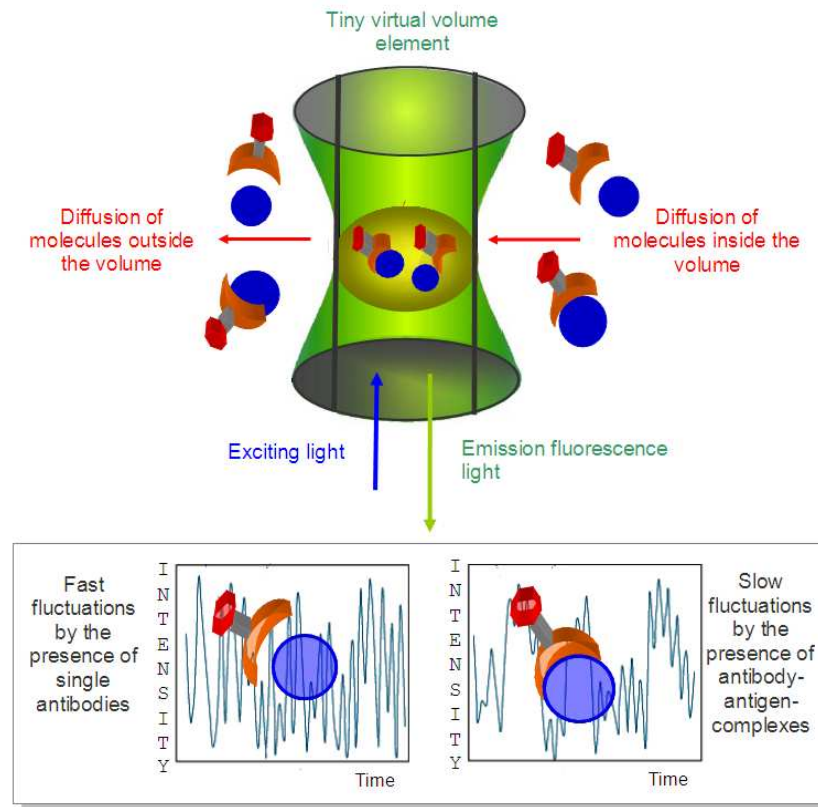


Figure 8. Shown is the diffusion of the labelled antibodies and the antigen-antibody complexes through the volume element, formed by the laser beam. The diffusion of the molecules through the volume element, due to their Brownian motion, is measured as fluctuations of the emitted fluorescence light. The different diffusion velocities give rise to different fluctuations lengths.

The function $W(r)$ is decayed to e^{-2} at r_0 in lateral direction and for $z = z_0$ in axial direction. By assuming the three dimensional Gaussian distribution of the emitted fluorescence light, the effective focal volume is calculated by:

$$V_{eff} = \int_V W(r) dV = \left(\frac{\pi}{2}\right)^{\frac{3}{2}} r_0^2 z_0 \quad (10)$$

The dimensions r_0 and z_0 are determined by calibration measurements (Figure 7). Integrating out the differential equation for the free diffusion yields:

$$c(r, t) = \frac{c_0}{8(\pi Dt)^{\frac{3}{2}}} \exp\left(-\frac{r^2}{4Dt}\right) \quad (11)$$

This leads to a relation between the diffusion constant and the concentration fluctuation:

$$\langle \delta c(r, t) \delta c(r, t + \tau) \rangle = \langle C \rangle \exp\left(-\frac{|r - r'|^2}{4D\tau}\right) \quad (12)$$

For the model of free diffusion, the auto-correlation function (formula 6) can be calculated analytically (by use of formula 8 and formula 12) as:

$$G(\tau) = G(0) \frac{1}{\left(1 + \frac{\tau}{\tau_D}\right)} \frac{1}{\sqrt{1 + \left(\frac{r_0}{z_0}\right)^2 \left(\frac{\tau}{\tau_D}\right)}} \quad (13)$$

τ_D is the diffusion time. This is the mean transit time of the molecule in the volume element (reciprocal of the average diffusion speed of the molecules). The relationship between the diffusion time τ_D and the diffusion coefficient D is given by:

$$\tau_D = \frac{r_0^2}{4D} \quad (14)$$

The auto-correlation amplitude $G(0)$ is proportional to the reciprocal of the average number of molecules $\langle N \rangle$ in the volume element:

$$G(0) = \frac{1}{\langle N \rangle} \quad (15)$$

Then, the local concentration of the fluorescent molecules in the effective focal volume element (formula 10) can be determined from the amplitude $G(0)$ of the auto-correlation function:

$$\langle C \rangle = \frac{\langle N \rangle}{V_{eff}} = \frac{1}{V_{eff} G(0)} \quad (16)$$

Due to statistical averaging, the relative fluctuations of the fluorescent signal become weaker with an increasing concentration of molecules. Therefore it is important to minimize the concentration of molecules in the focal volume. The decay of the auto-correlation function is determined by the diffusion time (Figure 9). When the correlation time τ equals the diffusion time τ_D , then the auto-correlation takes the form:

$$G(\tau = \tau_D) = \frac{G(0)}{2} \frac{1}{\sqrt{1 + \left(\frac{r_0}{z_0}\right)^2}} \quad (17)$$

The diffusion time τ_D is determined as fit parameter from the auto-correlation curve. Every augmentation of the mass of a biomolecule, resulting from the interaction with a second molecule, can be determined from the increase of the diffusion time. Molecular interactions are followed up by recording successive auto-correlation curves with shortest integration time. From those auto-correlation curves, changes in the diffusion time are determined (Figure 9).

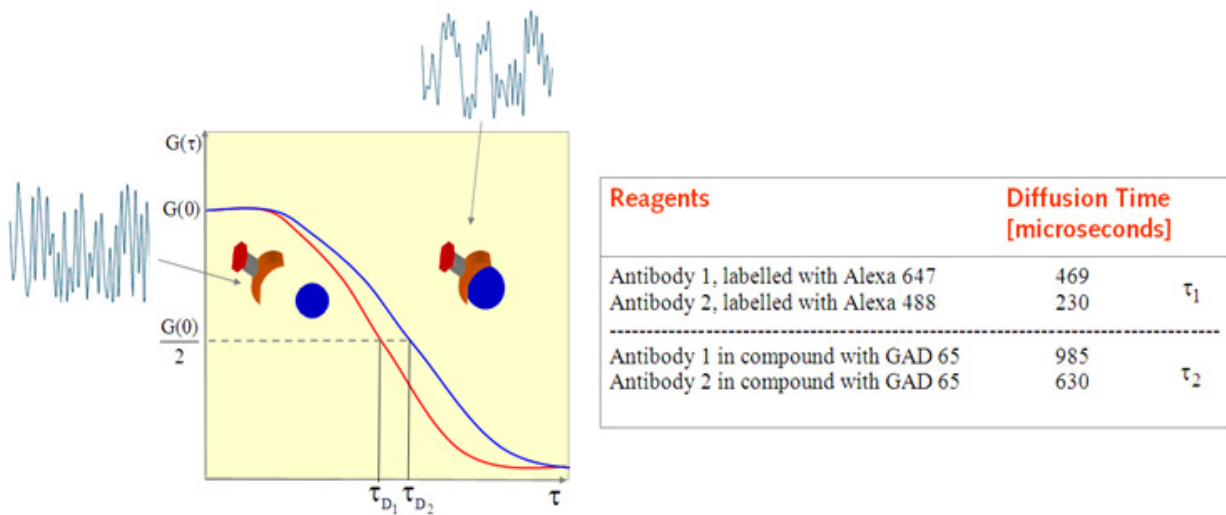


Figure 9. The diffusion time τ_D of the molecules is determined as fit parameter from the decay of the auto-correlation function $G(\tau)$. The interaction of the GAD 65 molecule with its antibody can be determined from the increase of the diffusion time.

2.1.4. Experiments

The sensitivity of the FCS method for the detection of GAD 65 was determined in clean and spiking experiments. Alexa 647 and Alexa 488 were used as dyes. In order to avoid disturbing auto-fluorescence for standardization, the detection of GAD 65 was carried out in bi-distillate water. By step-wise dilution, a minimal precisely detectable amount of 2.65 microgram/ml of GAD 65 was measured in such clean systems. To verify the minimal precisely detectable amount in sera, normal healthy controls were used, where the same amount of GAD 65 as to the clean systems was added (spiking experiment). Sera from 27 juvenile patients were investigated. All the children between 5 and 12 years were diabetes mellitus type 1 patients in an early stage and already had auto-antibodies. 126 sera of adult persons from normal admissions to the clinic served as controls. The sera from the paediatric patients came from a serum bank (Department of Paediatrics of the Medical University of Graz), the adult sera were fresh.

2.2. Enzyme-Linked ImmunoSorbent Assay (ELISA)

The second assay for the detection of the antigen GAD 65 in sera is the enzyme-linked immunosorbent assay (ELISA). As a heterogeneous assay, ELISA separates specifically components in a mixture by adsorbing them onto a solid phase which is physically immobilized. Therefore, the linking and adsorption of proteins (for example antibodies and antigens) is necessary. The chemical linking of proteins was developed by S. Avrameas and G. B. Pierce. The adsorption of proteins at solid states was developed in 1966 by L Wide and J.Porath. Based on these results, ELISA was developed in 1971 independently by two working groups, namely by P. Perlmann and E. Engvall at Stockholm University in Sweden and A. Schuur and B. van Weemen in the Netherlands [44,45]. There exist different types of

ELISA which differ in more or less steps: the 'indirect' ELISA, the 'sandwich' ELISA, the 'competitive' ELISA and the 'multiple' ELISA. One of the most useful and common of the immunoassays for the detection of antigens is the two antibodies 'sandwich' ELISA. This assay enables it to determine fast and accurately the antigen concentration in biological sera [46-48].

2.2.1. Principle and experimental setup

The sandwich ELISA requires two monoclonal antibodies, the capture and the detection antibody, that bind to different epitopes on the antigen. A microtiter plate (with a size of 127.76 mm×85.48 mm×14.35 mm) is a flat plate with multiple wells, arranged in a regular 8x12 matrix array, which serve as small test tubes. Each well holds tens of nanolitres to several millilitres of liquid. The capture antibodies are fixed to the wells of the microtiter plate (Figure 10). In a first step, the serum is added to the capture antibodies and the corresponding antigen is picked up (Figure 10). The unbound substances are washed away. In the next step, the detection antibodies are added and bind to the antigen. The detection antibodies are labelled with an enzyme. Again the enzyme-linked antibodies that do not bind are washed away. The remaining molecules form a "sandwich" consisting of layers of antibody/antigen/enzyme-linked antibody (Figure 10). In the last step, a colorimetric substrate is added, which is digested by the enzyme. This reaction results in a change of colour in the substrate, producing a visible signal, which indicates the quantity of antigen in the sample. Then, as result, the antigen is present in the sera if the substrate changes colour. The substrate concentration is measured by a photometer, whereby the concentration of the substrate is proportional to the antigen concentration in the serum.

2.2.2. Evaluation of the results, calculation of the calibration curve

For the evaluation of the ELISA output, the extinction is measured as a function of the concentration c of the coloured substrate inside the wells. The extinction E_λ is a measure for the diminishing of the intensity of light, with a wavelength λ , after passing a medium:

$$E_\lambda = -\ln\left(\frac{I}{I_0}\right) \quad (18)$$

I_0 is the intensity of the incident light, I is the light intensity after passing the medium. If the extinction values are applied on the y-axis and the logarithm of the concentration $\ln(c)$ on the x-axis, there results a sigmoid curve (mathematical function with an S-shape curve, including one turning-point and two asymptotes). Prior to the calculation of the calibration curve by a linear regression, the sigmoid curve must be transformed into a linear curve. The logit-function L is used for the linearization of sigmoid curves, which is of great importance for the evaluation of ELISA curves. From this operation results a linear curve. First, the measured extinction E_λ values are normalized so that the resulting values lie in the range between 0 and 1. The normalized extinction values are then expressed as:

$$N_E = \frac{E_\lambda - l_a}{u_a - l_a} \tag{19}$$

Whereby the upper (u_a) and lower (l_a) asymptotes of the sigmoid curve are used. The normalized extinction values are put into the logit-function L:

$$L = \ln\left(\frac{N_E}{1 - N_E}\right) \tag{20}$$

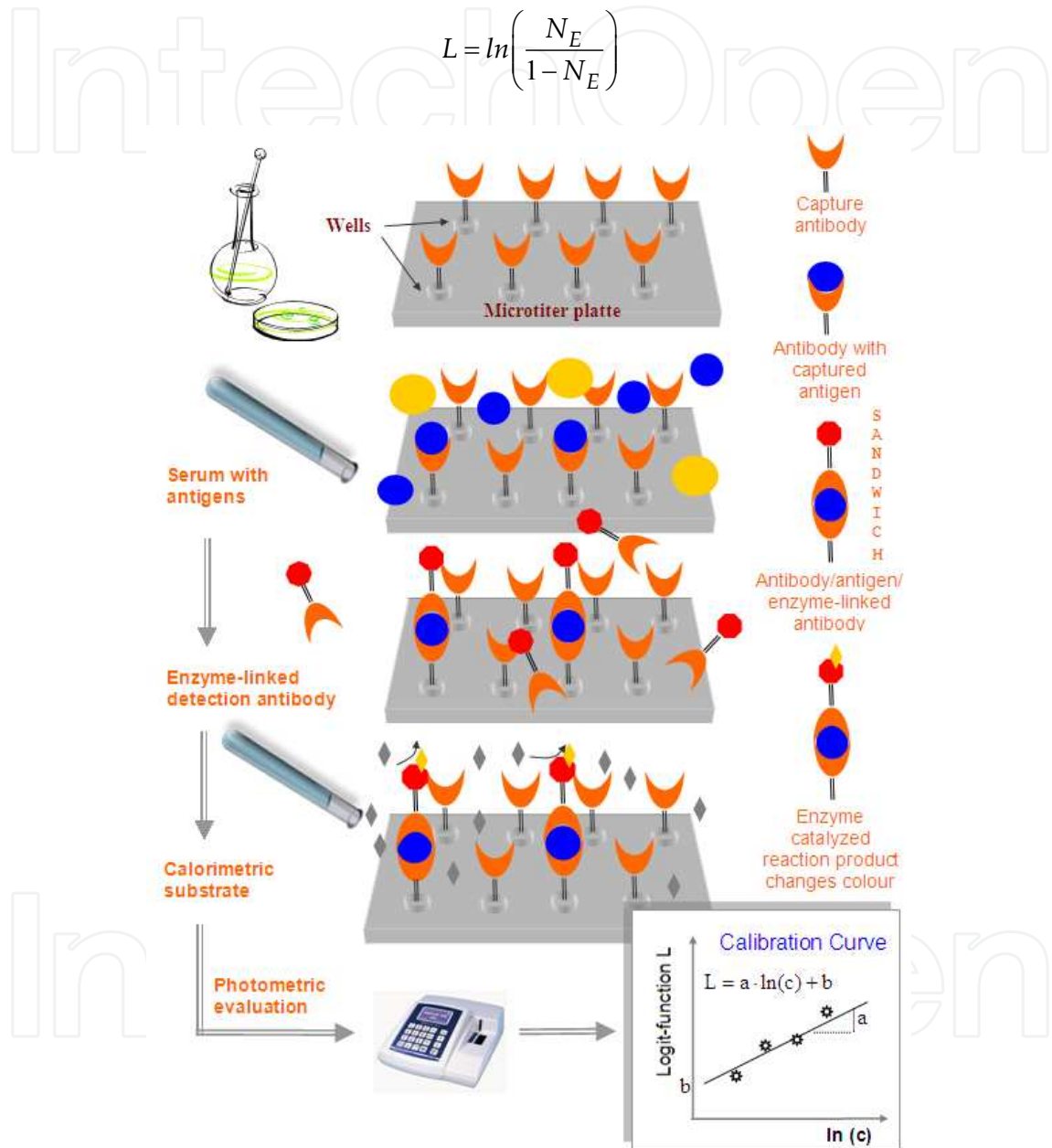


Figure 10. The capture antibodies are bound on a microtiter plate. The serum is added and the antigen GAD 65 is picked up. Then, the detection antibodies, labelled with an enzyme, are added and bind to the antigen. The enzyme catalyses a substrate reaction, whereby results a change of colour which is measured quantitatively by a photometer.

The value pairs of the logit-log-plot (x-value is the logarithm of the substrate concentration and the y-value is the logit of the normalized extinction values) are used for the linear

regression. From the linear regression results the high (b) and ascent (a) of the linear calibration curve:

$$L = a \ln(c) + b \quad (21)$$

Where: $\ln(c)$ is the x-value and L is the y-value (Figure 10). Then, the concentration c of the substrate is calculated out of the measured extinction values. The best accuracy is obtained in the neighborhood of the turning-point of the sigmoid curve, because in this range the ascent has a maximum value.

2.2.3. Experiments

In order to evaluate the stability of the GAD 65 molecule in sera, the concentration measurements in the samples were repeated after a time delay. Additionally the correlation between the GAD 65 concentrations from samples stored at different temperatures was determined. The correlation between the GAD 65 concentrations at different time steps is calculated by linear regression. Given a series of N measurements of the variables y_n and x_n ($n=1,2,\dots,N$), then the correlation coefficient R is applied to quantify the strength of their linear dependence:

$$R = \frac{\sum_{n=1}^N (x_n - \bar{x})(y_n - \bar{y})}{(N-1)\sigma_x\sigma_y} \quad (22)$$

The quantities \bar{x} and \bar{y} are the mean values of x and y and σ_x and σ_y are the respective standard deviations. If the coefficient equals 1, then the concentrations are completely linearly correlated. If the coefficient equals 0, then the variables are completely independent. Serum samples from 64 persons representing a cross-section of the samples in a blood bank (in Freiburg, Germany) were used. The specimens were randomly selected. Each sample was stored at room temperature and additionally in a refrigerator cooled at -80°C .

2.3. Surface Enhanced Laser Desorption Ionisation – Time Of Flight (SELDI-TOF)

Mass spectrometry is an analytical technique that measures the mass-to-charge ratio of charged particles. Based on preceding works of B. Goldstein and W. Wien, J.J. Thomson developed the first mass spectrograph [49]. End of the 1950's the mass spectrometry was applied to the analysis of amino acids and peptides. K. Tanaka developed the laser desorption which was applied for the ionization of biological macromolecules, especially proteins [50]. In this study mass spectrometry was carried out according to the surface enhanced laser desorption ionisation – time of flight (SELDI-TOF) system. SELDI-TOF has been proven as suitable tool in the clinical laboratory for the profiling of biomarkers in complex biological specimens such as: serum, plasma, intestinal fluid and urine [51-56].

SELDI-TOF consists of an aluminium carrier, called the array, a laser unit and a system which measures the time of flight (TOF) of the molecules (Figure 11). The TOF system includes an electric field, induced by the acceleration potential, and a detector. Photomultipliers, avalanche diodes etc. are used as detectors.

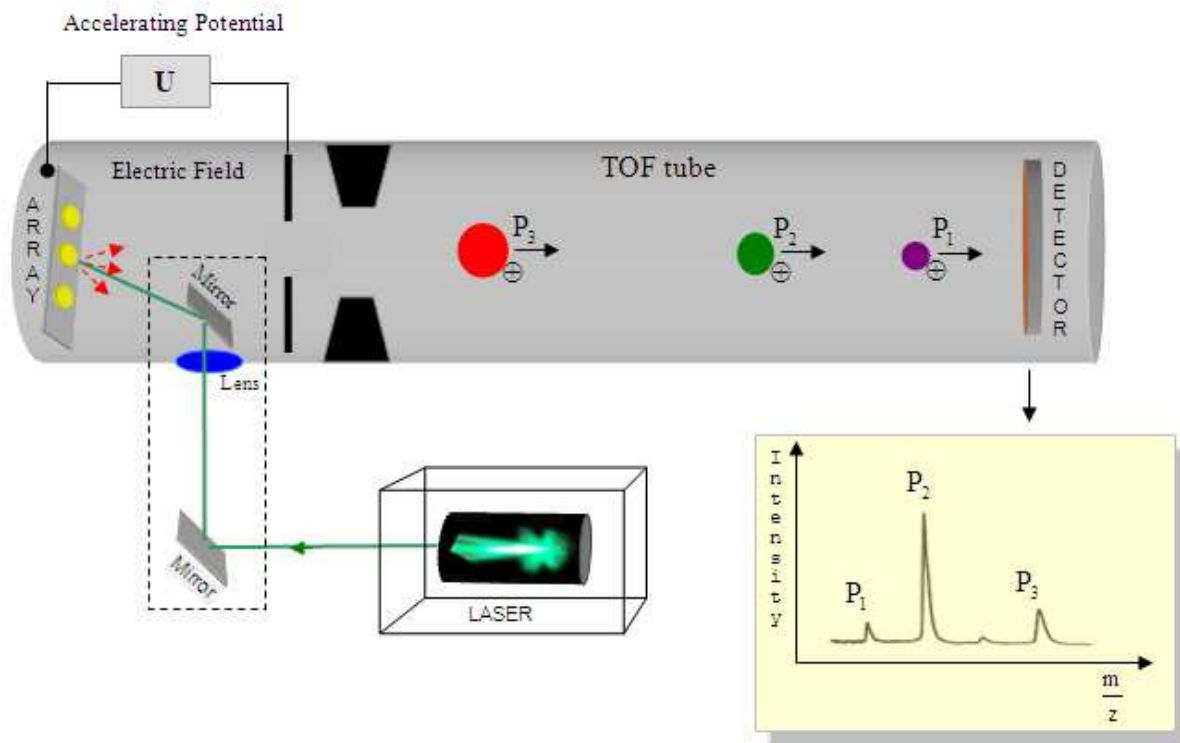


Figure 11. Surface enhanced laser desorption ionisation– time of flight (SELDI-TOF). The proteins are “eluted” from the matrix array by laser desorption and ionization. The ionized proteins are accelerated in the electric field and enter the TOF tube, according to their mass to charge ratio, with different velocities and each detection signal is represented by a peak in the mass spectrum.

2.3.1. Chip array

Proteins are captured by adsorption, electrostatic interaction, or affinity chromatography on the solid-phase protein chip array. The different chip types have either: surfaces that bind many different proteins or surfaces with a specific biomolecular affinity. The chips of the first type are composed of chemical surfaces, which have: hydrophobic, hydrophilic, anionic, cationic or metal affinity properties. The chips of the second type are composed of biochemically active surfaces, such as: immobilized antibodies, receptor proteins, DNA fragments or enzymes. The first type of surface binds many different proteins, whereas the second type binds only specific molecules, such as: antibodies, factors, DNA binding proteins and substrates. Therefore, the biochemically active surfaces are used to exploit specific molecular recognition mechanisms.

After putting the sample on the chosen chip type, the weakly bound molecules are washed away. The remaining sample molecules are mixed with small photosensitive molecules. These molecules cause the sample to crystallize and form the matrix as it dries. (The matrix

is composed of the molecules in the sample mix which are not analyzed). The photosensitive molecules facilitate desorption and ionization of the proteins in the mixture.

2.3.2. Laser desorption and ionization

The chip with the samples is put into a vacuum chamber, the flight tube of the mass spectrometer (Figure 11). The laser pulse excites the photosensitive matrix molecules. The energy of the excited molecules is converted into thermal energy which heats up the sample spot. The overheated part of the sample mix explodes into a plume and the molecules are liberated from the array (Figure 12). The protein molecules in the plume collide with the excited matrix molecules, whereby the matrix molecules transfer protons to the proteins and create charged proteins. Due to repeated processes, the proteins can get multiple charges.

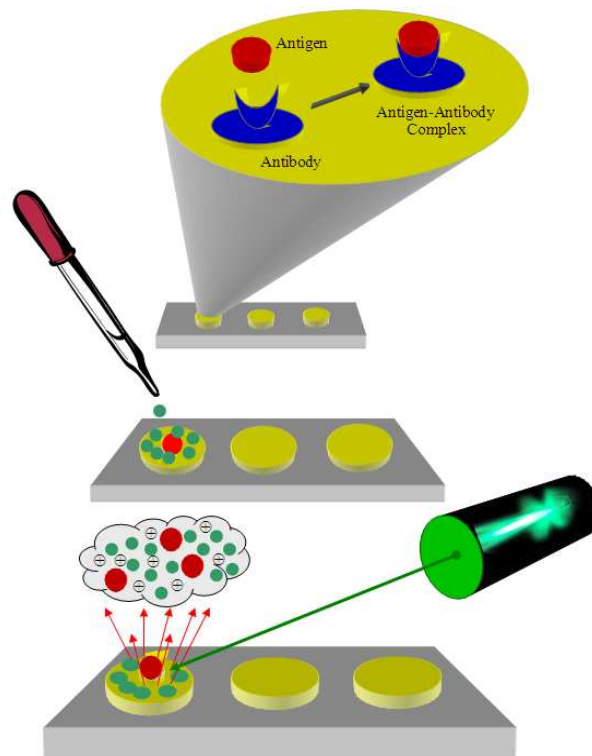


Figure 12. The chip array (aluminium carrier) contains immobilized GAD 65 antibodies, enabling it to focus specially on the GAD 65 antigen. The sample molecules are mixed with small matrix molecules, facilitating desorption and ionization of the proteins in the mixture. The laser pulse excites the matrix molecules; the serum molecules are liberated from the array and protonized.

2.3.3. TOF-measurement

Inside the vacuum chamber, an electric field (along the direction r) is generated by an electrostatic accelerating potential U :

$$\vec{E} = -\frac{\partial}{\partial r} U \quad (23)$$

The electric field is switched on synchronously with the end of the laser pulse. The protonated molecules are then accelerated in the electrical field by a force:

$$\vec{F} = ze\vec{E} \quad (24)$$

Where z is the net charge of the ionized molecule and e is the elementary electron charge ($1.602 \cdot 10^{-19}$ C). The molecules are accelerated into a field-free region, the TOF tube (Figure 11). Inside the TOF tube, the ionized molecules move toward the ion detector. The physical principle of the TOF analyser is that proteins, which have a different mass over charge ratio ($\frac{m}{z}$) are accelerated differently and enter the TOF tube with different velocities. The ratio of each protein molecule is recorded on the basis of the time required to pass through the tube. A protein with a net charge z , which passes through a potential difference of U , acquires an energy of:

$$E_{Pot} = zeU \quad (25)$$

The net charge is always a multiple whole number of the elementary electron charge e . The potential energy is converted, during the acceleration of the charged protein, into kinetic energy:

$$\frac{m}{2}v^2 = zeU \quad (26)$$

Where m is the protein mass and v is its velocity. Then the velocity of the protein inside the TOF tube equals:

$$v = \sqrt{\frac{2zeU}{m}} \quad (27)$$

Because the molecules gain the same kinetic energy in the electric field, the velocity of the molecules with a small mass is bigger than the velocity of molecules with greater masses. If the TOF tube has a length of d , the time of flight to the detector is given by:

$$t_{TOF} = \frac{d}{v} \quad (28)$$

The introduction of the molecule velocity (formula 27) into the equation yields:

$$t_{TOF} = \sqrt{\frac{m}{2zeU}} d \quad (29)$$

Then, the mass over charge ratio can be expressed as a function of the time of flight of the molecule:

$$\left(\frac{m}{z}\right) = \left(\frac{2eU}{d^2}\right)(t_{TOF})^2 \quad (30)$$

The detector measures the time interval between the switch on of the electric field and the moment a charged molecule hits the detector. When the molecules strike the detector plates, the plates release a certain multiple of electrons. The release of electrons is generally amplified by a cascade of successive releases (avalanche effect). The detector signal is then defined by the ratio of released electrons and the number of molecules striking the detector plate.

2.3.4. Mass spectrum and calibration

The counted totals per time interval are displayed in the spectrum (Figure 11). The detection of molecules with the same molecular weight and the same electric charge produce a signal which is called a singleton peak. A peak in the spectrum is then the signal induced by neighbouring singleton peaks. The peak area is proportional to the number of detected molecules. The baseline of the spectrum is formed by the dark current inside the detector and the detected air molecules. In practice, linear deviations from the expected (theoretical) relation are observed. Therefore a calibration must be performed before the measurement. The calibration equation is given by:

$$\left(\frac{m}{z}\right) = \alpha U (t_{TOF} - t_0)^2 + \beta \quad (31)$$

The calibration equation considers the linear deviation in the spectrum by inserting the extraction delay t_0 and the calibration parameters α and β . The parameter α is given by:

$$\alpha = a \left(\frac{2e}{d^2}\right) \quad (32)$$

The factor a is a temporary dummy variable. By measuring the time of flight t_{TOF} of molecules with well known masses, the calibration parameters α and β are determined.

2.3.5. Experiments

The sera were tested on a PS20 slide provided by Phadia, Sweden-Diagnostic, Freiburg/Breisgau, Germany. PS20 Protein chip arrays are 8 spot chips with 2 mm diameter spots, spatially compatible with one column of a standard 96-well microplate. The investigations were made with the CIPHERGEN system (CIPHERGEN Protein Chip Software 3.0) and the calibrations of the spectra were realized in point of view of the GAD 65. The serum was applied on the array and covered with the matrix from the laboratory of the Pasteur Institute in Paris. In a first experiment, sera without dilution were used and in a second experiment, the sera were diluted. To realize a diagnostic procedure, every serum was tested in duplicate with different successive dilutions (1:5, 1:10, 1:20.). Within the latter of "marker molecules" with known molecular weight such as Albumin and the analytical GAD 65 molecule purisimum and in spiking experiments, the existence of GAD 65 can be estimated. The concentration of albumin in sera is of course tremendously higher than the

concentration of the expected GAD 65. By use of the protein chip PS20 with fixation by covalent bonds of the GAD 65 antibodies, the contamination of the exuberant albumin is less disturbing. The sera from 2 paediatric patients (also contained in the sample set of the FCS measurements) with early onset of diabetes mellitus type 1 were kindly provided from the serum bank of the Department of Paediatrics of the Medical University of Graz.

3. Results

3.1. FCS

Clean and spiking experiments allowed a minimal precisely detectable amount of the GAD 65 at the concentration of 2.65 microgram/ml. The measured diffusion times are shown in figure 9. This enabled a sufficient serum dilution and avoids interference by auto fluorescence and other proteins in the FCS system. With diffusion times of 985 resp. 630 microseconds, GAD 65 could be found in 8 sera from patients with diabetes in an early onset. 4 of the patients were juvenile patients and 4 were adults, which were initially used as controls, who retrospectively showed signs of autoimmunity.

3.2. ELISA

GAD 65 was found in different concentrations, where the values range from 0.10-514.7 ng/ml (1 ng/ml = 10^{-9} g/ml), in all the samples (Figure 13). This leads to an average concentration of 58.00 ng/ml. The correlation between the GAD 65 concentrations from samples stored at room temperature and the same samples stored in a refrigerator cooled at -80°C are shown in Figure 14.

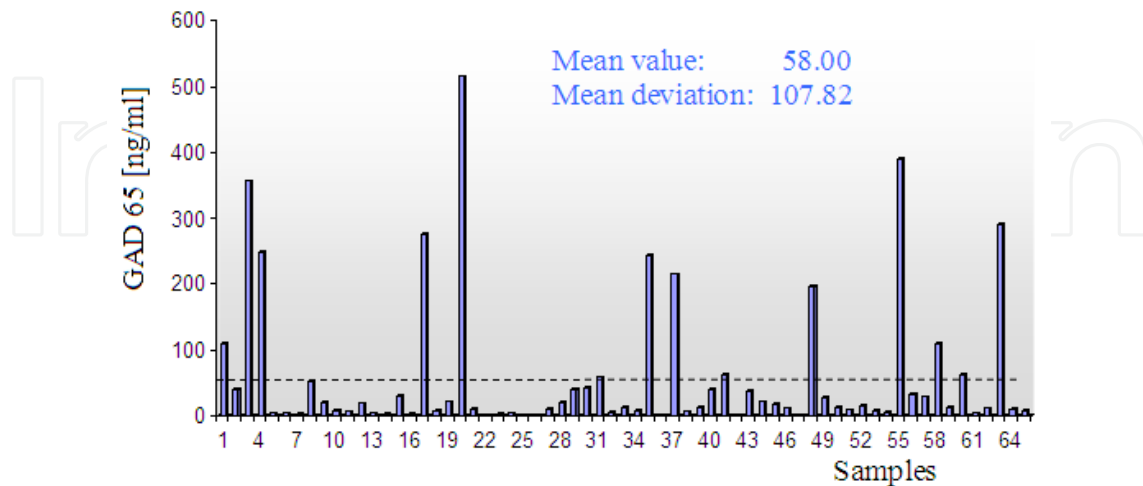


Figure 13. With the ELISA setup, GAD 65 was found in human sera from a blood bank, with values ranging from 0.10-514.7 ng/ml.

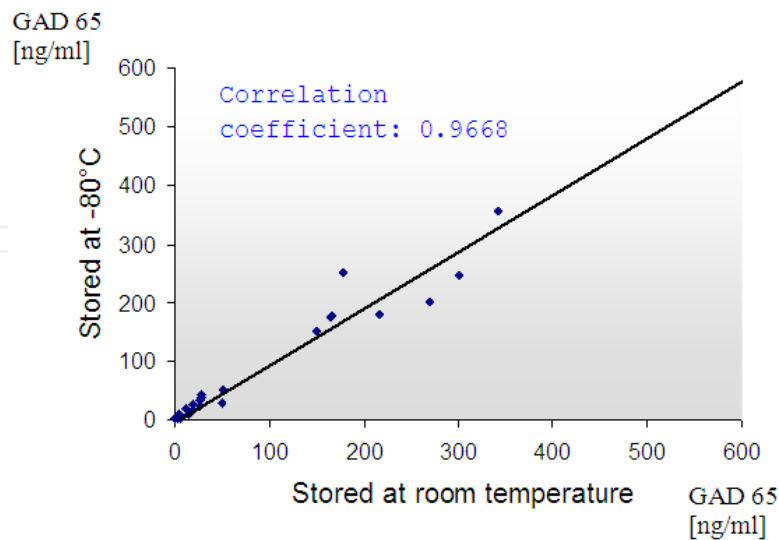


Figure 14. Correlation between the GAD 65 concentrations from samples stored at room temperature and cooled at -80°C .

The high value of the correlation coefficient (0.9668) shows that there is practically no difference in the concentrations between samples at room temperature and the same samples at -80°C . Additionally, the correlation between the GAD 65 concentrations taken from samples stored at room temperature and taken from the same samples after a time delay of one week was calculated. During this week, the samples were stored at room temperature (Figure 15). The value of the correlation coefficient (0.9897) demonstrates that the GAD 65 molecule remains highly stable over a time period of one week.

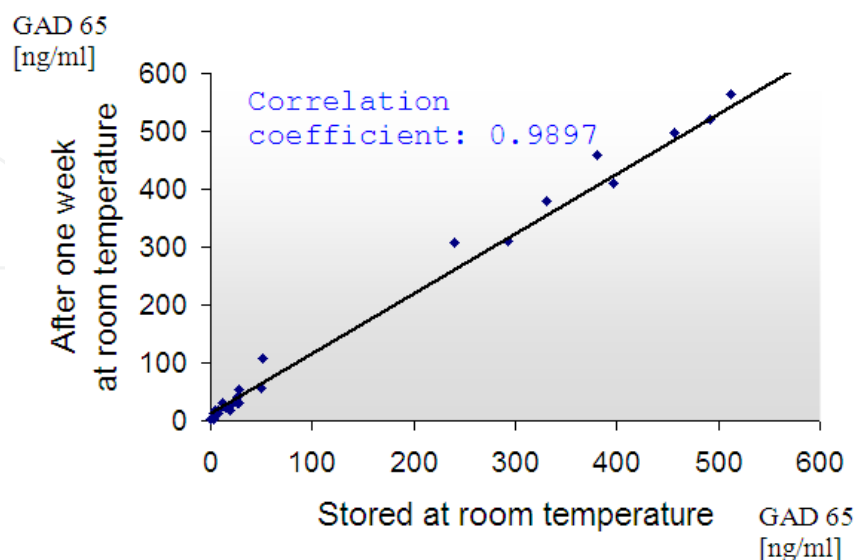


Figure 15. Correlation analysis between the GAD 65 concentrations taken from samples stored at room temperature and taken from the same samples after a time delay of one week.

3.3. SELDI-TOF

Evidence for GAD 65 in one serum sample in the mass spectrum was found, giving a peak very close to albumin with a molecular weight of 65 kDa. This serum was from a juvenile patient with an early onset of diabetes mellitus type 1. Peak evaluation after spiking experiments was done to have comparable results as with FCS. The spectra always show the peaks of the antibodies at 50, 75 and 150 kDa. The spectra of the diluted sera (Figure 16) show a much diminished peak of the reference albumin. For the interpretation of the results, the peak intensity at 65 kDa was calibrated in proportion to the intensity of the albumin peak in the reference. The intensity of the appropriate peak in the spectrum is greater than the peak obtained for albumin by a factor of 8.4.

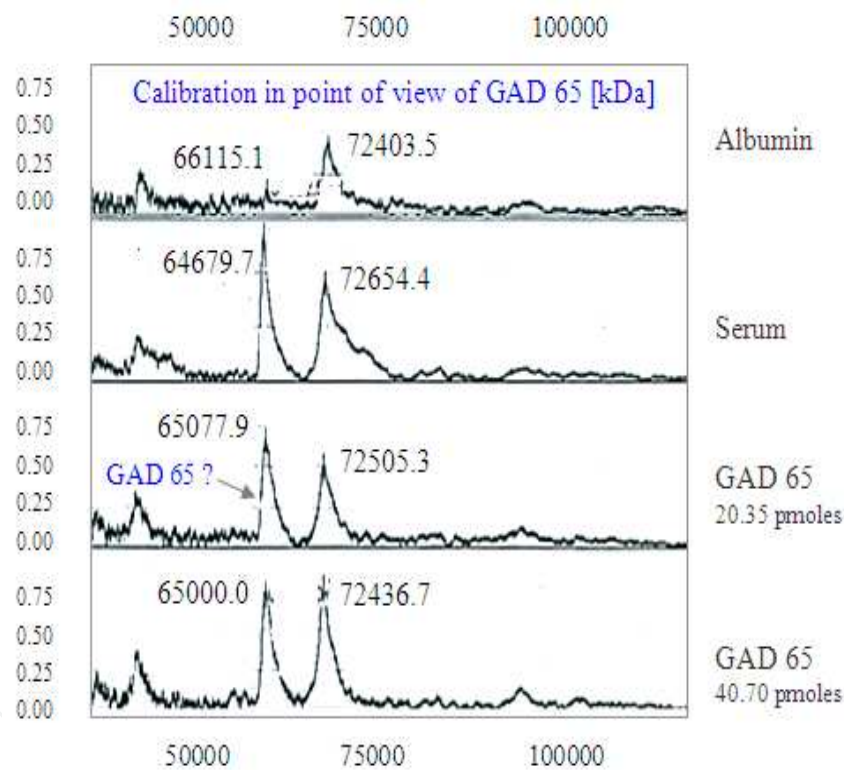


Figure 16. The sera are diluted at 1:20. The spectrum of the diluted serum shows a peak at 65kDa which may result from GAD65. The intensity of the peak is greater, by a factor of 8.4, than the corresponding albumin peak. This serum is from a paediatric patient with diabetes mellitus type 1 at an early stage.

4. Molecular analysis and visualization

Functional specificity and biological function of a protein are linked to its structure. Due to the 3-D folding structure, the residues, which are responsible for the protein function, are brought into a precise geometric arrangement. The rest of the protein structure is mainly necessary to enable and maintain the correct spatial position between the amino acids on the

active site. Therefore, to understand a protein function, the 3-D structure of the protein reveals far more information than its sequence.

For an analysis and planning of neutralization of GAD 65 with antibodies in the sera, the locations and shapes of the epitopes on the GAD 65 molecule are important. The structural visualization of the GAD 65 molecule and its epitope locations is illustrative and may help the reader to speculate on the antigenic sites of the molecule, enabling an understanding of the interaction with the immune-receptor, which is the basis for the development of active or passive immunotherapy in the near future. The epitopes are well known in literature and were identified by homolog-scanning mutagenesis, where segments of sequences from a homologous molecule (GAD 67) known not to bind to the specific antibodies are systematically substituted throughout the GAD 65 gene [57,58]. A complete or partial loss of antibody reactivity by the resulting mutated molecules (chimeras) suggests that GAD65 specific sequences required for contact with the antibody has been exchanged by the point mutation. The quaternary structure of GAD 65 was determined experimentally by X-ray diffraction [59]. In this paper the visualization is done with the Swiss-Pdb Viewer (<http://spdbv.vital-it.ch>) [60].

4.1. Visualisation of macromolecules

Bioinformatics is an interdisciplinary discipline between computer science and molecular biology. On one side, bioinformatics is a science with interconnected data banks, connecting sequence information to structural, biomedical and clinical data. On the other side, bioinformatics is a science which provides mathematical algorithms and computational tools for: detecting sequence similarities and finding homologous sequences; prediction, analysis and visualization of protein 3-D structure etc.

Structural information about proteins is available in the PDB structure database, an international repository for 3-D structure files [61]. Once a protein structure has been determined experimentally, either with crystallographic methods or by nuclear magnetic resonance spectroscopy, the structural information is deposited into the PDB. The structural information is stored in the PDB as data files, which contain mainly the Cartesian coordinates of all atoms involved in the protein (Figure 17). The entry point to the structural protein data is the PDB web site: <http://www.rcsb.org/pdb>. The database is accessed via Internet and the selected PDB data files, containing the atomic coordinates, are downloaded. The data files are used as input for protein visualization and the viewer software transforms the information in the PDB data file into an appropriate representation of the protein 3-D structure. Usually the molecules are visualized by “balls-and-sticks” models or by ribbons showing their secondary structures (Figure 5). The step from a molecule (set of connected atoms) to geometric shape is done by space filling diagrams. The theory of space filling diagrams is part of topology: the area of mathematics concerned with spatial properties that are preserved under continuous deformations of objects.

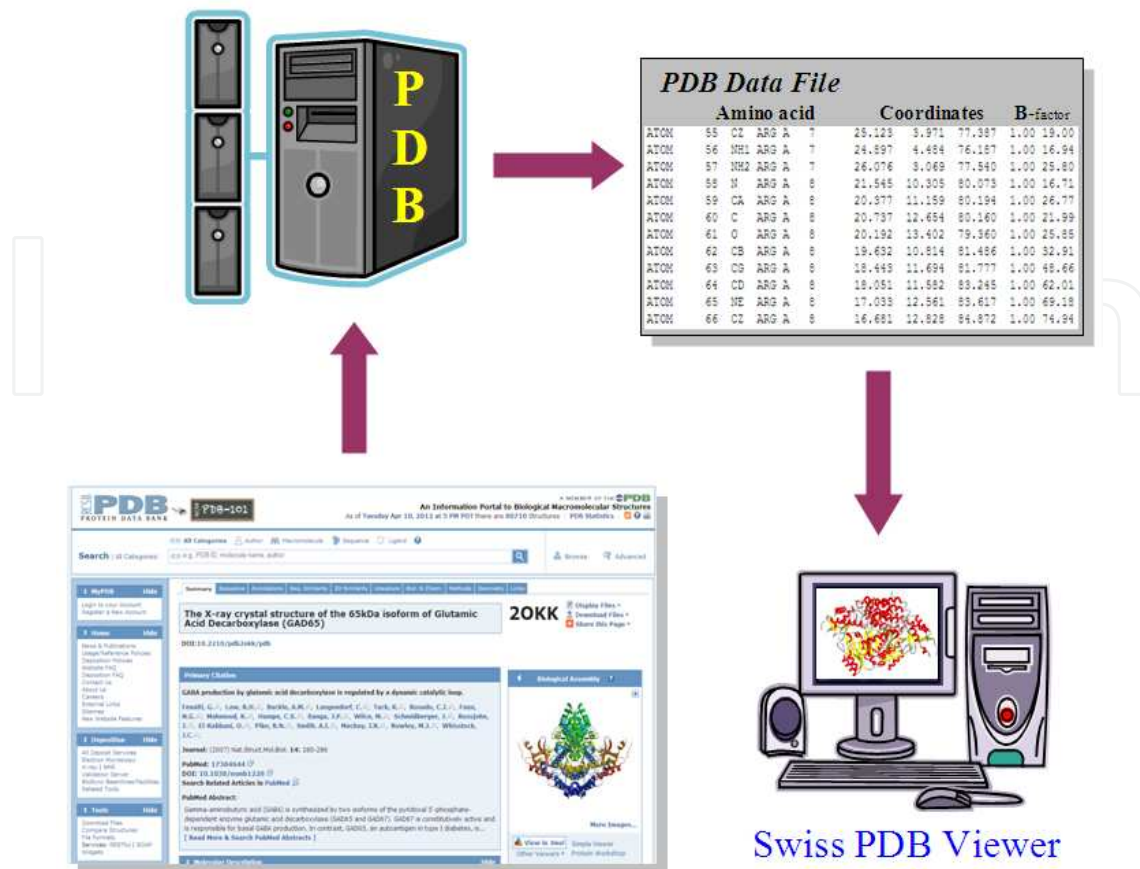


Figure 17. Protein structural information is available at the Protein Data Base (PDB). At the moment the database contains more than 80.700 experimentally determined structures. The PDB is contacted through the Internet. The structural information is stored in the PDB data files as atomic coordinates. The B-factor indicates the precision of each atom position. The requested PDB data files are downloaded and the protein structure visualized locally.

4.2. Space filling models and molecular shapes

Space filling diagrams are models that represent a molecule by the space it occupy [62-65]. They are embedded in the 3-D space (\mathbb{R}^3) and show properties that make them suitable for molecular analysis. Each atom in a space filling diagram is represented by its location in space and a quantitative expression of influence on its surrounding. Most commonly, the space-filling diagram of a molecule is defined as the union of overlapping balls A_i :

$$SFM = \bigcup_{i \in \mathbb{N}} A_i \quad (33)$$

The molecular boundary is defined as the envelope of the union of overlapping spheres. Three types are of special interest: the van der Waals model, the solvent accessible model and the molecular surface model.

Van der Waals model (VW): Due to the movement of the electrons around the atomic nucleus, an atom can be considered as an electric dipole. The dipole of an atom polarises the

neighbour atom resulting in a transient attractive force between the atoms. Conversely, at short ranges a repulsive force between the electrons of both atoms arises. The radius at which the repulsive force begins to increase sharply is called the van der Waals radius. The van der Waals sphere A_i of the i -th atom of a molecule is specified by its atom type and has a location in space: $z_i \in \mathbb{R}^3$ and a radius $r_i \in \mathbb{R}_+$. This radius r_i is the same for all atoms of the same type i . The van der Waals model of a molecule is a union of balls:

$$VW = \left\{ x \in \mathbb{R}^3 \mid \exists_i : \|x - z_i\| \leq r_i; i = 1, \dots, N \in \mathbb{N} \right\} \quad (34)$$

N is the number of atoms in the molecule. That means: the van der Waals model is the set of points x which are located inside the distance r_i from the centre of the van der Waals sphere A_i . The van der Waals spheres of binding atoms overlap, whereas the spheres of non-binding atoms do not overlap (Figure 18). As the van der Waals model, the following space filling models depend on the atomic van der Waals radii and the coordinates of the atoms in the molecule.

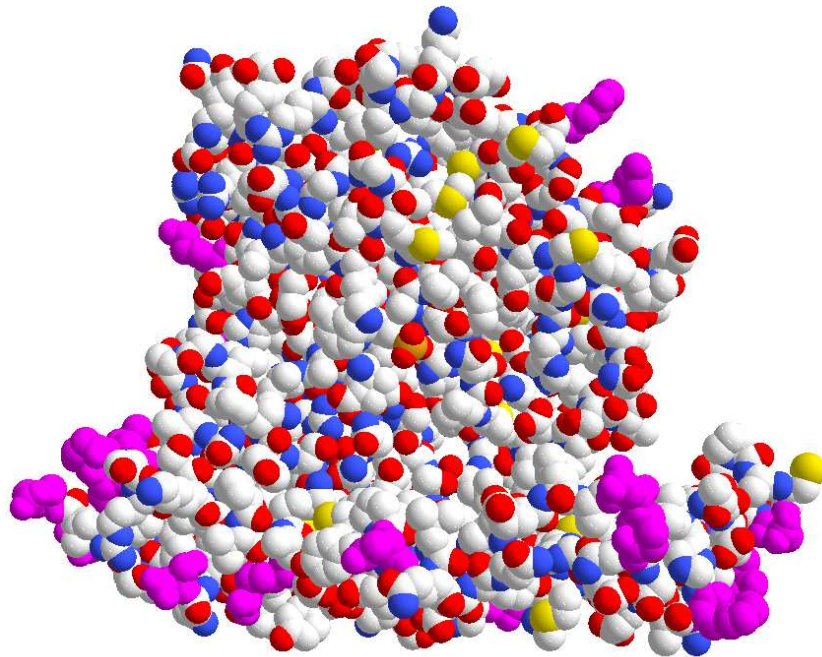


Figure 18. Van der Waals surface of GAD 65: The boundary of the space filling diagram is made up as envelope of the union of spheres with van der Waals radii.

Solvent accessible model (SA): The interaction of the Van der Waals model and a solvent molecule, represented as sphere of radius ρ , is studied by increasing the radius r_i of every van der Waals sphere, associated to an atom A_i , by ρ . That means: the radius of the van der Waals sphere is expanded by the radius of the solvent (Figure 19). The solvent accessible model is then defined (similar to the van der Waals model) as the union of the enlarged balls:

$$SA = \left\{ x \in \mathbb{R}^3 \mid \exists_i : \|x - z_i\| \leq r_i + \rho; i = 1, \dots, N \in \mathbb{N} \right\} \quad (35)$$

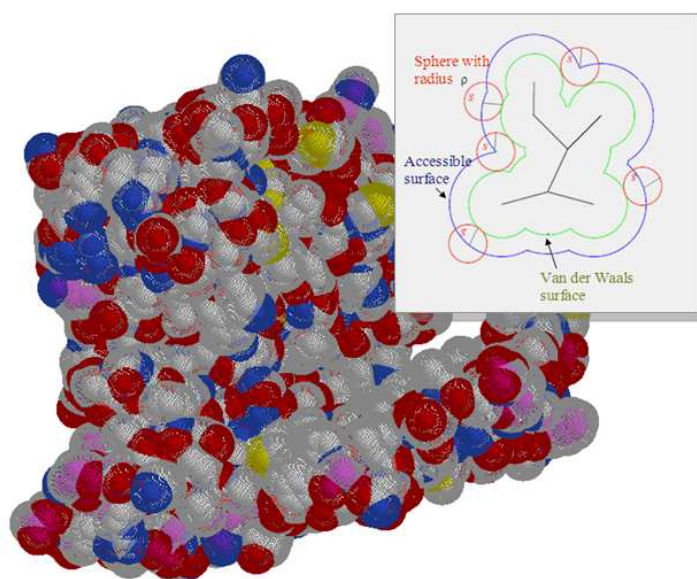


Figure 19. Solvent accessible model of GAD 65: The boundary of the space filling diagram is made up as union of spheres which are grown by the radius of the sphere of a single solvent molecule. The accessible surface is the surface generated by the centre of the solvent sphere rolling of the van der Waal surface.

The accessible surface is the surface generated by the centre of the solvent sphere rolling of the van der Waals surface. The radius ρ of the solvent sphere is usually set to 1.4 angstrom (the approximate radius of a water molecule).

Molecular surface model (MS): A model that resembles in size the van der Waals model and in connectivity the solvent accessible model is the molecular surface model. It consists of all points $x \in \mathbb{R}^3$ that lie outside all solvent spheres disjoint from van der Waal modell:

$$MS = \left\{ x \in \mathbb{R}^3 \mid \forall_{y \in SA} : \|x - y\| > \rho \right\} \quad (36)$$

The surface is generated by a sphere of radius ρ rolling about the van der Waals model. The molecular surface is the envelope generated by the rolling sphere. It differs from the van der Waal surface by covering portions of the volume inaccessible to the rolling sphere (Figure 20). It consists of sphere and torus patches connected in a tangent continuous manner. The shape of a molecule is described by the molecular surface, which is the boundary of the molecule volume within which no other molecule can enter. The molecular shape of the antigen and the corresponding antibody is of special importance for the understanding of their intermolecular interaction. The interaction is usually described in terms of locks and keys: The shape of the lock (the antigen) must be complimentary to the shape of the key (the antibody) to initiate an immune response. The body develops antibodies with the right shape to attack specific antigens. The docking places for the antibodies are the epitopes of the antigen. The locations of the sequence fragments, constituting the epitopes, are highlighted on the GAD 65 3D structure (Figure 21). Molecular surfaces are suitable for the visualization of the epitope shapes, which enables a pictorial analysis of the local docking sites and their fitting. For the quantification of the epitope accessibility to the paratopes of the antibodies, dual models of the space filling diagrams are used.

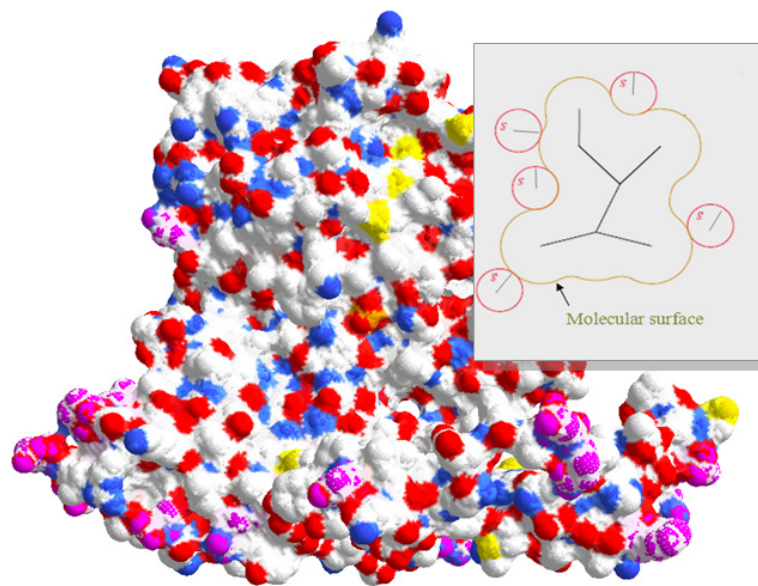


Figure 20. Molecular surface of GAD 65: Boundary that is obtained by rolling the solvent sphere over the van der Waals surface. The molecular surface is the envelope generated by the rolling sphere. It consists of sphere and torus patches connected in a tangent continuous manner and filling up the inaccessible crevices and cusps.

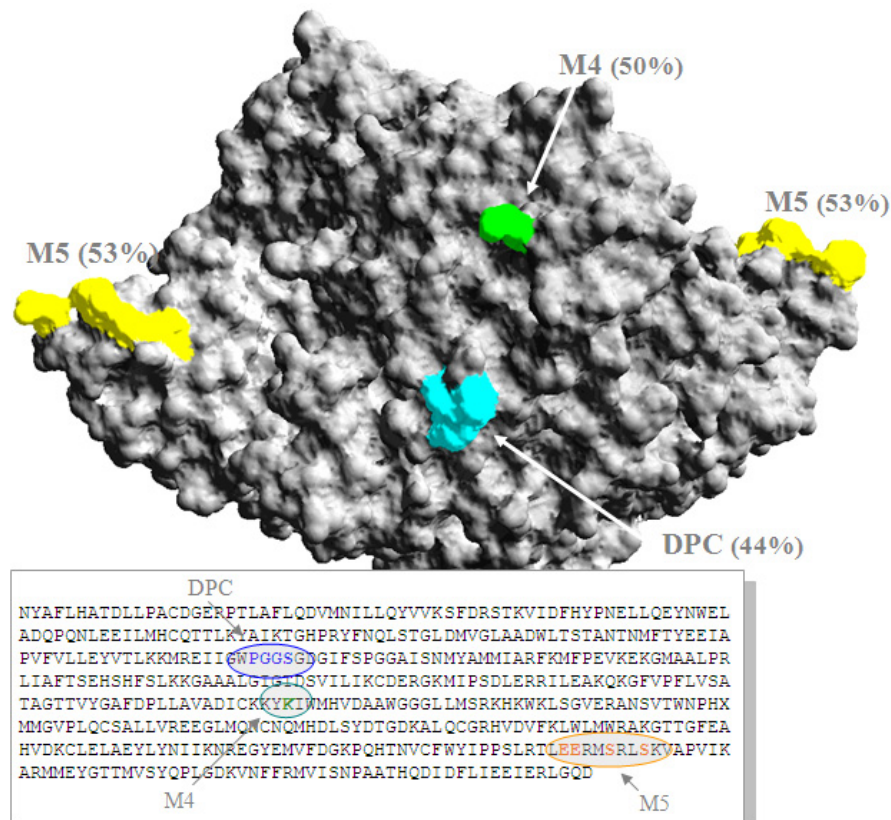


Figure 21. The GAD 65 molecule is represented by its molecular surface. The shapes of the GAD 65 epitopes, enable a pictorial analysis of the local docking sites. The exposure values of the residues, constituting the epitopes, were calculated by Voronoi tessellation. These values (in %) indicate how much the epitopes are exposed to the surrounding solvent, indicating the accessibility to potential antibodies.

4.3. Dual models and exposure values

The space filling models have a common dual counterpart. The dual counterpart is constructed by the Voronoi diagram that decomposes the union of balls (VW or SA model) into convex pieces [66-68].



The weighted distance of a point $x \in \mathbb{R}^3$ from A_i is defined as:

$$\pi_i(x) = \|x - z_i\|^2 - r_i^2 \tag{37}$$

The Voronoi cell V_i of A_i is the region of points whose weighted distance to A_i is as least as small as to any other ball:

$$V_i = \left\{ x \in \mathbb{R}^3 \mid \forall_j : \pi_i(x) \leq \pi_j(x) \right\} \tag{38}$$

Each Voronoi cell is an intersection of closed half-spaces and therefore a convex polyhedron. Any two Voronoi cells overlap at most along some piece of their boundary and together the collection of cells covers the entire \mathbb{R}^3 . The common intersection of $k + 1 > 1$ Voronoi cells is either empty or a common (3-k)-dimensional face. In Voronoi tessellation, the space, containing a set of discrete points P_l , is subdivided into the non overlapping Voronoi cells [68]. Each cell V_l is associated with an element of the set of points P_l in that way, that every region contains space points x , which have the shortest distance to the associated point:

$$V_l = \left\{ x \in \mathbb{R}^3 \mid \|P_l - x\| < \|P_k - x\|, l \neq k \right\} \tag{39}$$

This partition of the space is called Voronoi tessellation. In the definition, the Euclidean metric is used as measure:

$$\|P_k - x\| = \sqrt{\sum_{i=1}^3 |P_k - x_i|^2} \tag{40}$$

For a given set of points the Voronoi decomposition is unique. The set of Voronoi cells is called a Voronoi diagram, which defines the topological relations of the set of discrete points (Figure 23A). The Voronoi tessellation describes the space filled by a packing of solid polyhedrons, connected by their faces, without empty space between them. The configuration of the cells provides information about the package of the associated set of points. Each cell in the diagram is characterized by its number of edges and faces (Figure 22). All the values concerning the individual cells, such as: cell volume, cell surface, number

of sides, number of faces, area of contact faces and distances between the representative points, are derived from the geometry of the tessellation.

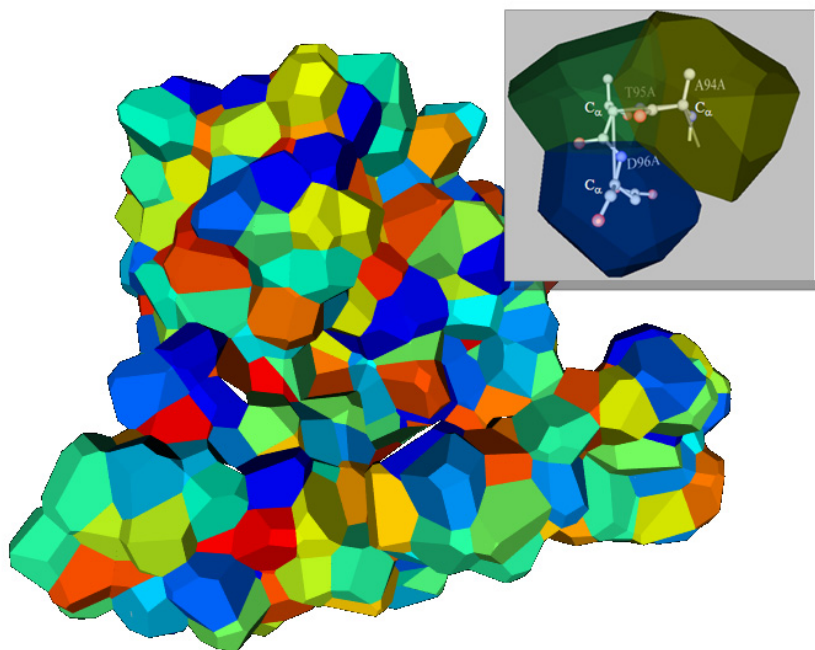


Figure 22. Voronoi tessellation of the GAD 65 molecule. Each Voronoi cell V_i is a polyhedron which is uniquely associated with one of the residues. The C_α atoms are used as centre points. Each cell in the Voronoi diagram is characterized by its number of edges and faces. The common faces of the cells define the contacts with nearest residues.

For completeness, let us shortly introduce the Delaunay triangulation. The Delaunay complex is a collection of simplices that records the overlap pattern among Voronoi cells. The complex contains the convex hull of $k+1$ ball centres if their corresponding Voronoi cells have a non-empty common intersection. Let B be a subset of $k+1$ atoms with $Z_B = \{z_i | A_i \in B\}$ and $V_B = \{V_i | A_i \in B\}$. Then the Delaunay complex is:

$$D = \left\{ \sigma = H_{conv}(Z_B) \mid \bigcap V_B \neq \emptyset \right\} \quad (41)$$

Where $(H_{conv}(Z_B))$ denotes the convex hull of the points in Z_B . Figure 23A shows a Voronoi tessellation of a set of 4 points in the plane. In 2-D the Voronoi cell of a point is given by a polygon, where the intersection of the contact lines is build with aid of the lines joining the neighbour points. The set of segments joining the points two by two is called Delaunay triangulation, which is the dual of the Voronoi diagram (that means that it represents the same geometrical information about the set of points).

A Voronoi tessellation can be used to quantify the contact areas of individual residues in proteins. The tessellations are mostly performed on the alpha carbon atoms (as point P_i) of the structure. The tetrahedron set, sharing a particular alpha carbon C_α as a vertex, defines its closest neighbourhood. The circumscribed sphere of each tetrahedron does not contain

any other alpha carbon (Figure 22). Two residues are in direct contact if their corresponding cells share a common face. To obtain quantitative values for the epitopes area, the exposure rate of the epitopes to the surrounding solvent was calculated. The contribution of an amino acid, at the epitope, to the exposure rate, is characterized by the number and size of the faces of its Voronoi cell exposed to the solvent. The total area of the Voronoi cell V_l of the l -te residue is denoted by F_l . The area of the i -te common face to the solvent is: a_i . N_a is the number of common faces. Thus a measure for the exposure of the l -te residue to the solvent is the relative exposure value:

$$E_l = \frac{1}{F_l} \sum_{i=1}^{N_a} a_i \quad (42)$$

The total area of the epitope can be quantified by summing up the areas for all the involved residues. Then, the contribution of the l -te residue of the epitope is given by the relative contribution:

$$I_l = \frac{E_l F_l}{\sum_j E_j F_j} \quad (43)$$

The relative exposure values (in %) of the epitope residues give hints about the accessibilities of the antibodies to the GAD 65 molecule and are shown in Figure 21. The Voro3D software was used for the Voronoi tessellations (<http://www.lmcp.jussieu.fr/~mornon/voronoi.html>) [69].

4.4. Molecular electronic states and molecular recognition

The structural visualization of the GAD 65 molecule and its epitopes, together with their electrostatic field, is illustrative and may help the clinical immunologist to better imagine the mechanisms of the GAD 65 antigenicity. The specific antigen-antibody recognition and the attraction of the two molecules are done by the electrostatic fields surrounding the molecules. The electrostatic potential can be studied locally at the epitopes or globally, surrounding the whole molecule at different distances. The local electrostatic potential generated by the epitope residues, at the epitope location play a role in the recognition and adjustment of the antibody at the docking place. The global electrostatic potential is extending in the surrounding solvent influencing other molecules.

The electron behaviour in molecules is treated by methods based on quantum theoretical calculations. The Hamiltonian operator for the electronic Schrödinger equation describes the dynamic of the involved electrons [70-72]. For a molecule with N electrons and K nuclei, the Hamiltonian operator is given by:

$$H = -\sum_{i=1}^N \frac{\hbar^2}{2m} \Delta_i - \sum_{i=1}^N \sum_{a=1}^K \frac{Z_a e^2}{r_{ai}} + \sum_{i=1}^N \sum_{\substack{j=1 \\ j>i}}^N \frac{e^2}{r_{ij}} \quad (44)$$

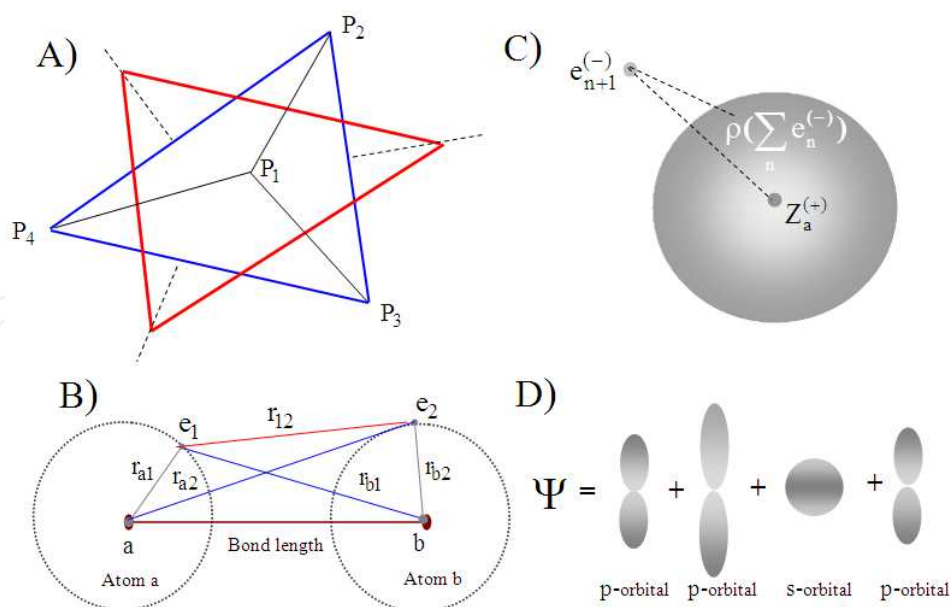


Figure 23. A) Voronoi tessellation (red) of a set of 4 points in the plane together with the dual Delaunay triangulation (blue). B) The interactions between the electrons e and nuclei a, b of a molecule. C) The independent electron moves in the electrostatic field of the nuclei and the averaged field of all other electrons. D) The molecular orbital Ψ is build as linear combination of atomic orbital.

The Hamiltonian operator involves the kinetic energy of the N electrons (first term: $\hbar = \frac{h}{2\pi}$, h is Planck's constant $6.626 \cdot 10^{-34}$ Js) the interaction of the electrons with the K nuclei (second term), the electron-electron interactions (third term). Z_a is the nuclear charge in atom a , r_{ai} is the distance between electron i and nucleus a , r_{ij} is the distance between electron i and electron j (Figure 23B). Then the electronic properties are calculated with the nuclei coordinates as parameters which are provided by the corresponding PDB data files. The resulting major part of the further calculation remains in solving the electronic Schrödinger equation:

$$H\Psi_n = E_n\Psi_n \quad (45)$$

The only possible values for the energy in quantum theory are the eigenvalues E_n of the Hamiltonian operator in the Schrödinger (eigenstate) equation with eigenfunctions Ψ_n . A significant simplification can be obtained by introducing an independent-particle model where the dynamic of an electron is considered to be independent of all other electrons and the interaction is taken into account in an average fashion. That means that the electron moves independently in the electric field of the nuclei and the field of all other electrons (Figure 23C). In the independent-particle model, the total state function Ψ of a molecule with N electrons is the product of the N single electron state functions Ψ_k ($k=1, \dots, N$). In quantum theory, the values of an observable are the expectation values of the corresponding operator in pure (eigenstates) or mixed states (linear combination of eigenstates). The energy of a molecular system, described by an appropriate state function, is therefore calculated as the expectation value of the Hamiltonian operator (in Dirac bra-ket notation):

$$\begin{aligned}
 E &= \langle \Psi | H | \Psi \rangle \\
 &= \int \Psi^*(r_i) H \Psi(r_i) dV
 \end{aligned}
 \tag{46}$$

The energy of the molecular system, in the independent-particle model, is then given by:

$$\begin{aligned}
 E &= \sum_{k=1}^N \langle \Psi_k(i) | h_i | \Psi_k(i) \rangle \\
 &+ \sum_{k=1}^N \sum_{\substack{l=1 \\ l>k}}^N \left[\langle \Psi_k(i) \Psi_l(j) | h_{ij} | \Psi_k(i) \Psi_l(j) \rangle - \langle \Psi_k(i) \Psi_l(j) | h_{ij} | \Psi_l(i) \Psi_k(j) \rangle \right]
 \end{aligned}
 \tag{47}$$

The first expression describes the mean kinetic energy of the electrons and the potential energy in the electrostatic field of the nuclei.

$$\langle \Psi_k(i) | h_i | \Psi_k(i) \rangle = \int \Psi_k^*(r_i) \left[-\frac{\hbar^2}{2m} \Delta_i - \sum_{a=1}^K \frac{Z_a e^2}{r_{ai}} \right] \Psi_k(r_i) dV_i
 \tag{48}$$

The second term describes the Coulomb interaction between 2 electrons, where one electron is located in the k -orbital and the second in the l -orbital (the charge is distributed inside the orbitals).

$$\langle \Psi_k(i) \Psi_l(j) | h_{ij} | \Psi_k(i) \Psi_l(j) \rangle = \iint \Psi_k^*(r_i) \Psi_k(r_i) \frac{e^2}{r_{ij}} \Psi_l^*(r_j) \Psi_l(r_j) dV_i dV_j
 \tag{49}$$

The third term describes the exchange interaction resulting from the indistinguishability of the electrons (this is a pure quantum effect and has no classical analogue).

$$\langle \Psi_k(i) \Psi_l(j) | h_{ij} | \Psi_l(i) \Psi_k(j) \rangle = \iint \Psi_k^*(r_i) \Psi_l^*(r_j) \frac{e^2}{r_{ij}} \Psi_l(r_i) \Psi_k(r_j) dV_i dV_j
 \tag{50}$$

Since molecular systems, involve the motions of a large number of electrons, their Schrödinger equations cannot be solved exactly and approximate solutions must be used. The molecular orbitals are expanded in terms of the basis functions, the atomic orbitals:

$$\Psi_n(r_i) = \sum_{\mu=1}^M c_{n\mu} \phi_{\mu}(r_i)
 \tag{51}$$

This expansion is called “Linear Combination of Atomic Orbitals” (LCAO). $\phi_{\mu}(r_i)$ are the well known atomic orbitals: s-orbital, p-orbital, d-orbital. The coefficients $c_{n\mu}$ define the contribution of the atomic orbital’s to the molecular orbitals and are the weight of the μ -the atomic orbital in the n -te molecular orbital (Figure 23D). These coefficients have to be

determined to find the molecular orbitals. Until now the molecules were considered as a system of electrons and nuclei, the expansion in atomic orbitals reflects the chemical view where molecules are building up of single atoms. The objective is now to find molecular orbitals that make the energy a minimum. This is done by determining a set of coefficients $c_{n\mu}$ that minimize the energy:

$$\delta E = \frac{\partial E}{\partial c_{n\mu}^*} = 0 \quad (52)$$

($c_{n\mu}^*$ is the complex conjugate of $c_{n\mu}$). The variation procedure yields the HF-LCAO (HF: Hartree-Fock) equation system (also called Roothan-Hall equations) for the coefficients:

$$\sum_{\beta=1}^M (H_{\alpha\beta} - \varepsilon_n S_{\alpha\beta}) c_{n\beta} = 0 \quad (53)$$

This is the most important equation in the quantum theory of molecules. $S_{\alpha\beta}$ is the overlap matrix:

$$S_{\alpha\beta} = \int \phi_{\alpha}^*(r_i) \phi_{\beta}(r_i) dV_i \quad (54)$$

The solutions of the HF-LCAO equation system are the energy ε_n ; ($n=1, \dots, M$) and the coefficients $c_{n\beta}$; ($\beta=1, \dots, M$) for the molecular orbitals Ψ_n ; ($n=1, \dots, M$). It is a linear equation system, of dimension $M \times M$, where the solutions for larger molecules highly depend on computer power. The dimension of the equation system depends on the number of atoms and the involved atomic orbitals. In the simplest version only the p-orbital's contributing to the delocalized π -bonds are considered (Hückel molecular orbitals), in a higher version all the valence orbitals contributing to the chemical bonds are used (Extended Hückel). In more sophisticated versions, beside the valence orbitals also inner atomic orbitals are used. The complexity of the equation system and the computational power depend on the evaluation of the integrals. The matrix elements of the Hamiltonian are given by:

$$H_{\alpha\beta} = \langle \phi_{\alpha}(i) | h_i | \phi_{\beta}(i) \rangle + \sum_{\rho=1}^M \sum_{\sigma=1}^M P_{\rho\sigma} \left[\langle \phi_{\alpha}(i) \phi_{\rho}(j) | h_{ij} | \phi_{\beta}(i) \phi_{\sigma}(j) \rangle - \frac{1}{2} \langle \phi_{\alpha}(i) \phi_{\rho}(j) | h_{ij} | \phi_{\sigma}(i) \phi_{\beta}(j) \rangle \right] \quad (55)$$

$P_{\alpha\beta}$ is the density matrix, which is defined by:

$$P_{\alpha\beta} = 2 \sum_{n=1}^{N/2} c_{n\alpha}^* c_{n\beta} \quad (56)$$

A principal difficulty in solving the HF-LCAO equations is the large number ($\sim M^4$) of two-electron integrals. These integrals can involve up to four atomic centres. Therefore calculations for large molecules require enormous computer power. Semi-empirical methods reduce the computational cost by neglecting all three-centre and four-centre two-electron integrals and the use of empirical parameters.

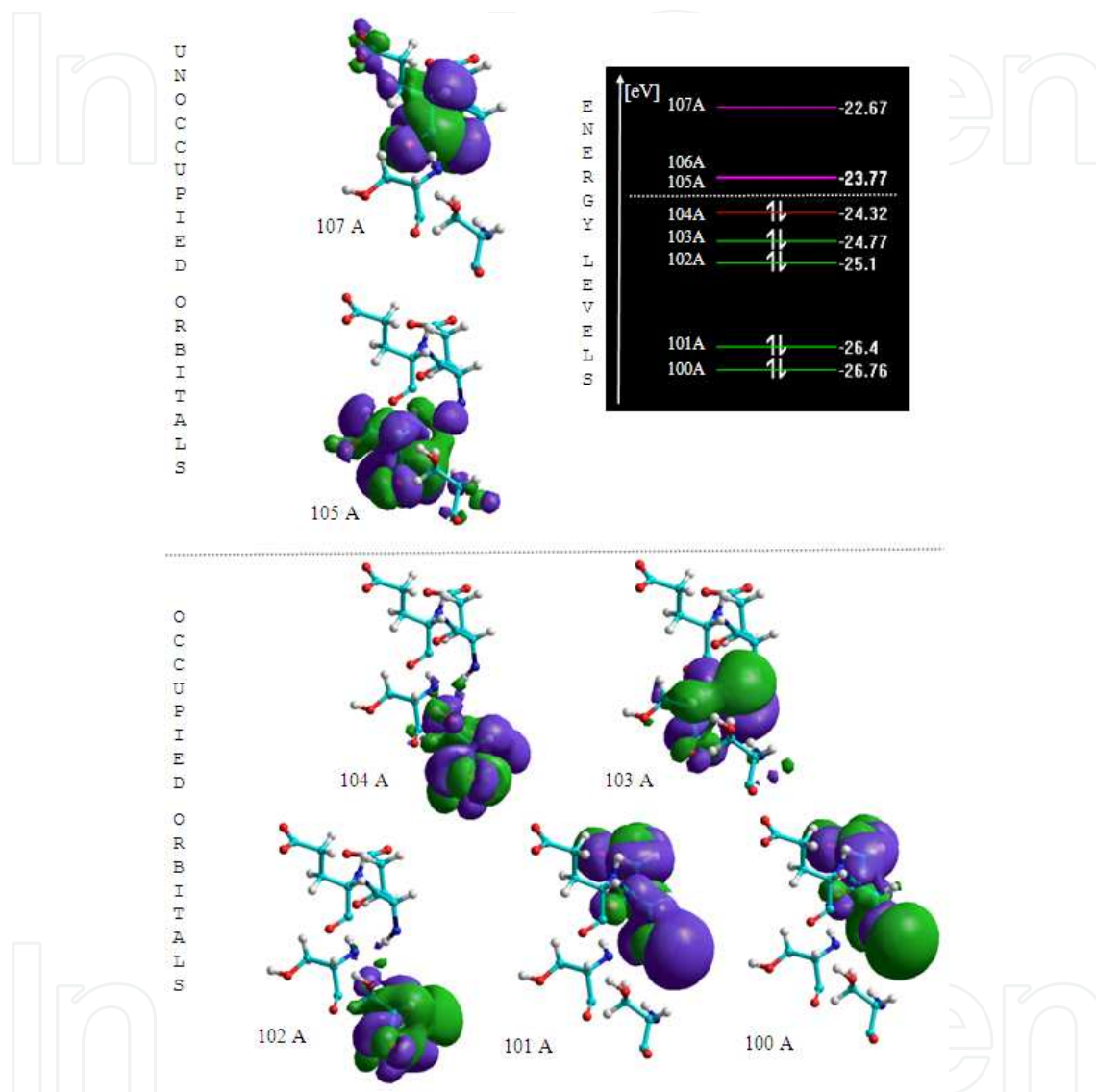


Figure 24. A subset of the molecular orbitals from the epitope M5 is shown together with their energy levels. Positive values of the molecular orbitals are green encoded, negative values violet. The most important orbitals in organic chemistry are the highest occupied molecular orbital (HOMO: 104 A) and the lowest unoccupied molecular orbital (LUMO: 105 A).

The molecular orbitals are arranged in order of increasing energy ϵ_n (Figure 24). Then the electrons are assigned to the orbitals beginning with the lowest energy. As a result, in a system with N electrons, the $N/2$ lowest molecular orbitals are occupied by respectively up to two electrons with opposite spins. The remaining $M-N/2$ (virtual) orbitals are unoccupied in the ground state and are occupied in excited electronic states (Figure 24). Physically, the

square of the orbitals represents the electron spatial density distribution or in other words: the probability for finding the electron in a certain space volume element. Because of the protein size, a full treatment on the quantum level is beyond the realm of the available computers. Therefore mixed quantum/classical (QM/MM) methods are chosen, whereby the GAD 65 molecule is divided into the epitopes, where a quantum description is required, and the rest of the molecule which is treated classically by molecular force fields (Figure 25). Once the molecular orbitals are known, a number of molecular properties can be calculated out of the molecular orbitals. The electron density is given by:

$$\rho(r) = \sum_n \Psi_n^*(r) \Psi_n(r) \quad (57)$$

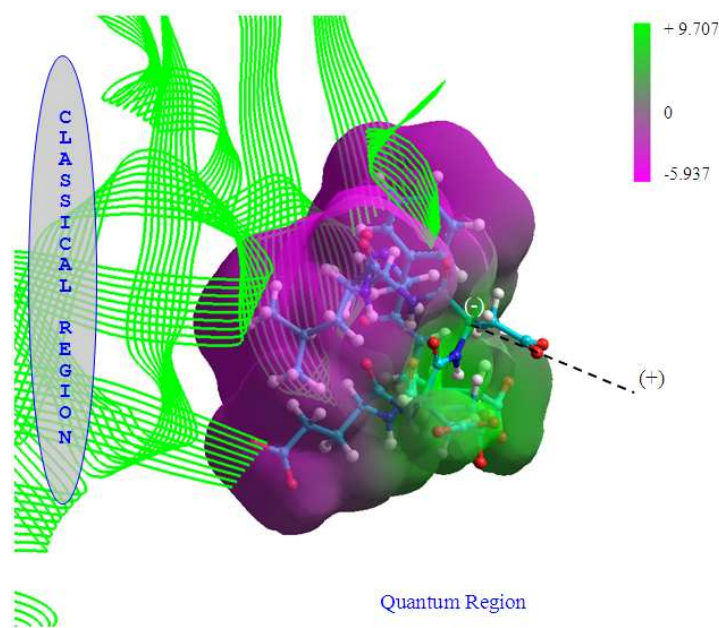


Figure 25. The electron density distribution at the residues of the epitope M5 is shown. The electron density in the visualisation is colour encoded according to its electrostatic potential. For large molecules, like GAD 65, the molecule is divided into a classical region and a quantum region. The epitope residues are treated by quantum mechanics and the rest of the molecule is treated classical by using molecular force fields. The spatial orientation of the dipole moment is shown (dotted lines). The surface shows electron density values of $8 \cdot 10^{-5} e / a_0^3$.

It describes the distribution of the electrons in the molecule (Figure 25). The values of the electron density are expressed in units of e / a_0^3 , where e is the electron charge and a_0 is the Bohr radius (0.5 angstrom).

The electrostatic potential $V(r)$ is expressed as an electrostatic potential map, showing constant contouring values.

$$V(r) = \sum_{a=1}^K \frac{Z_a}{|R_a - r|} - \int \frac{\rho(r')}{|r' - r|} dr' \quad (58)$$

The first part of the equation results from the electrostatic potential of the atomic nuclei (point charge at position R_a) and the second part from the electron distribution (Figure 25). The values of the electrostatic field are expressed in units of e/a_0 . The electrostatic field \vec{E} acts perpendicular on the potential surfaces. It is a measure of the force exerted between molecules. The electrostatic potential at the epitope location plays an important role in the specific antigen-antibody recognition e.g. the specific interaction of the antigen GAD 65 with antibodies (Figure 26). At greater distances, the charge distribution of the whole molecule is taken into consideration and the electrostatic potential attracts molecules in more extended ranges (Figure 27). The quantum mechanical calculations were done with HyperChem (<http://www.hyper.com>).

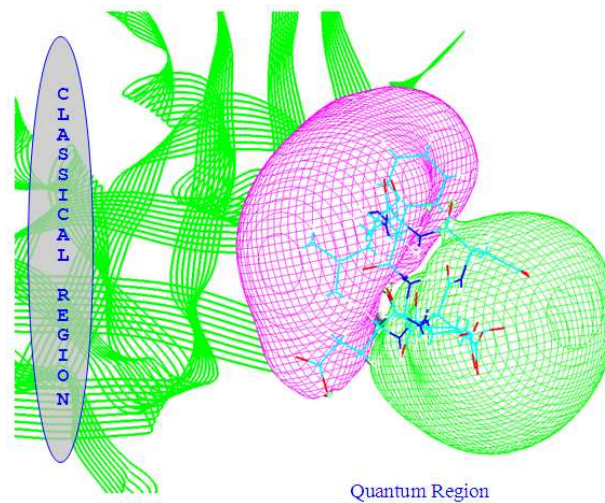


Figure 26. The spatial distribution of the electrostatic potential surrounding the residues of the M5 epitope. Negative values are red encode, positive values green. The surface shows where in 3D the electrostatic potential has a value of $3.8e/a_0$.

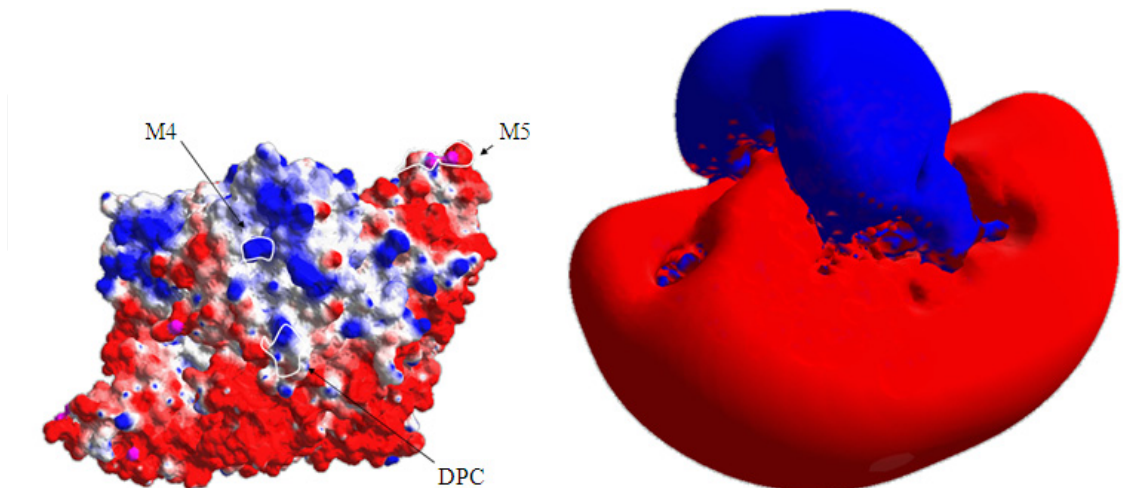


Figure 27. The electrostatic potential surrounding the GAD 65 molecule plays an important role in the specific antibody recognition. The electrostatic potential map shows contours of constant values. Positive potential values are drawn in blue, negative values in red. Different constant electrostatic potential values, ranging from the neighbourhood (left) to more extended ranges (right) are shown.

5. Discussion

The enzyme GAD 65 was generally considered to be strictly intracellular. But such a strictly intra-cytoplasmatic antigen would never have access to the immune system. With the ultrasensitive FCS technology, GAD 65 could be found to exist in peripheral blood of patients with diabetes mellitus type 1. It was measured with a sensitivity of 2.65 microgram/ml in the sera of adult and paediatric patients. The antigen was not found in all the patients' sera. The reason of the incidence is probably due to the complexed form (antigen-antibody complex) of GAD 65 at the time of investigation, hence hiding the antigen in the antibody excess. This could make it undetectable for FCS.

To understand the procedure and development of immunization and therefore the occurrence of GAD 65 antibodies in the blood, it was proposed that in an initial step the immune system is primed by the accessibility to GAD 65. The assumption was that the enzyme has to be in the human serum and should be found in higher concentrations before the onset of the disease. FCS is a very sensitive method, but the technique requires a labelling of the antibodies with dyes, which is very difficult to achieve and makes the measurements with FCS time consuming and expensive. Furthermore, the method is very sensitive to disturbance, resulting from other proteins (like albumin) and free dye contamination. Therefore and encouraged by the relative high concentration of GAD 65 in the blood of patients with diabetes mellitus type 1, we used in the following an ELISA setup. In the ELISA setup, the antigen GAD 65 was detected, in the peripheral blood of persons representing a cross-section of 64 samples in a blood bank. The result from the ELISA experiments demonstrates that GAD 65 exists, in mostly small amounts, in the sera of the blood-donors. The average concentration of GAD 65, by taking all these samples into consideration, is 58.00 ng/ml. By assuming that the most blood-donors are healthy, it can be expected that GAD 65 exists in at least small concentrations in the human peripheral blood. (For the diabetes mellitus type 1 patients the concentrations are by factors 40-50 higher). The correlation analysis of the samples stored at -80°C and additionally at room temperature showed that the GAD 65 molecule in the sera is stable at room temperature. By determining the correlation between the GAD 65 concentrations, taken from samples stored at room temperature and taken from the same samples after a time delay of one week, it was found that the molecule GAD 65 is sufficiently stable in sera.

By the use of SELDI-TOF and the study of some specimens used in the previous work with FCS we found some evidence for the diabetic antigen GAD 65 in a peak close to albumin. The albumin, produced in the liver, is the most abundant protein in human blood plasma. The reference range for albumin in blood is 35 to 53 mg/ml. Its concentration is therefore higher, by a factor above 10.000, than the expected value of GAD 65 (2.65 microgram/ml). The molecular weight of albumin is 66.47 kDa and therefore near the molecular weight of GAD (65 kDa). The weights differ only by 2.26%. Because of the tremendously higher concentration of albumin in the sera, a peak evaluation in regard of GAD 65 could not be achieved in a proper manner. Although an array with GAD 65 antibodies was used to pick

out the antigen of the sera, it seems that the omnipresent albumin could not be completely washed out, but remained partially on the chip bounded by van der Waals interactions. This leads to a superposition of the GAD 65 peak and the albumin peak at ≈ 65 kD, which complicate the proper detection of the antigen. The results of these first trials show that the application of SELDI-TOF for the detection of GAD 65 in human sera, in the manner presented here is not reliable for a routine procedure. In conclusion, the development of new techniques for the separation of GAD 65 from albumin is necessary for an accurate and reliable detection of the diabetes type 1 antigen.

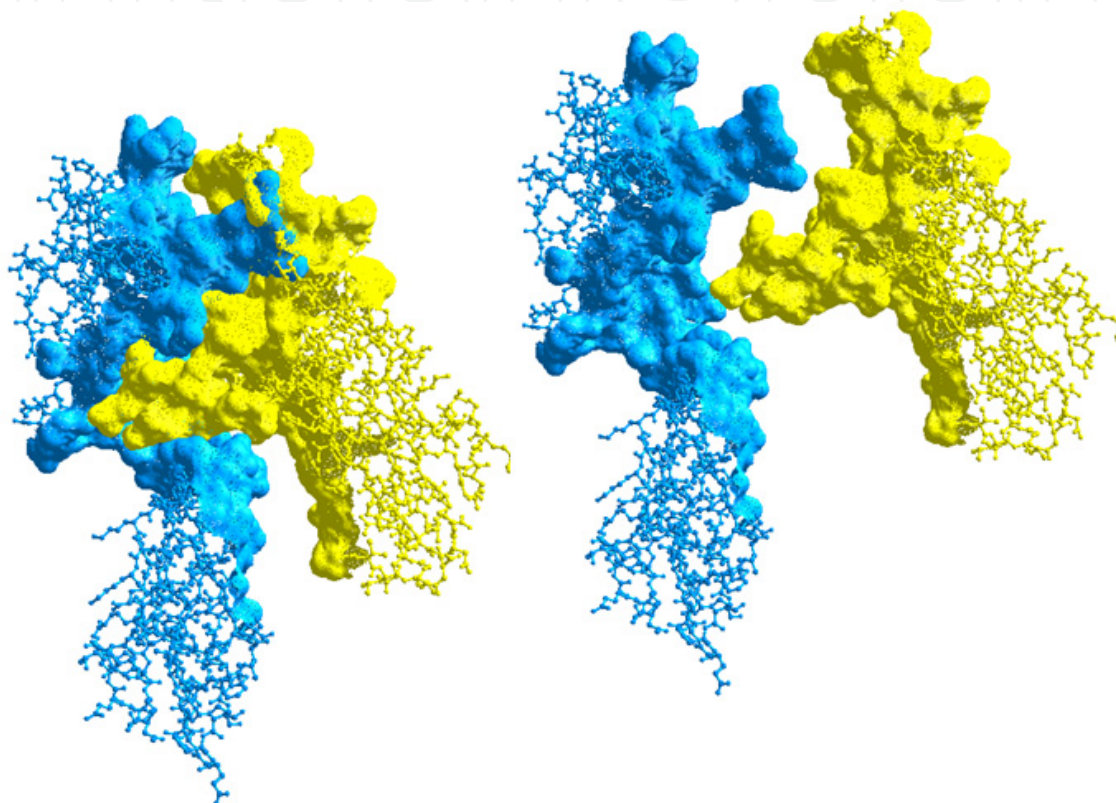


Figure 28. Interacting molecular surfaces. The major histocompatibility complex (MHC) protein (blue) I-Ag7 interacts with GAD 65.

The source of GAD 65 in serum of normal healthy human is unknown. Numerous hydrophobic parts at the protein surface enable a potential interaction with the hydrophobic membrane lipids, leading to a reversible anchoring of the molecule to the cell membrane. Another source may be the normal turn-over of beta cells. To explain the mechanism of autoimmunization, the visualization of the GAD 65 tertiary structure, together with its antigenic determinants and the associated electrostatic field, is essential. Molecular modelling enables an imagination of the GAD 65-antibody interaction and understanding of antigenicity and binding sites, which is the basis for the development of an active or passive immunotherapy [73]. The 3-D molecular surface, derived from space filling models, illustrates the fitting of the GAD 65 epitopes to the paratopes of the antibodies (GADA) and other associated molecules (Figure 28). It enables a pictorial understanding of the interaction

with the antibody via complementary surfaces. Quantitative values for the GAD 65 antigenic properties were obtained with Voronoi tessellation (dual model) by calculating the exposure rate of its epitopes to the surrounding solvent and the GAD antibodies. The electrostatic potential and details of the electronic structure of the GAD 65 epitopes were calculated by quantum theoretical methods. The specific antigen-antibody recognition and the attraction of the two molecules are done by the electrostatic fields surrounding the molecules. The local electrostatic field at the epitope location plays a crucial role in the antibody-antigen recognition.

6. Conclusion

Biomarkers are molecules which are associated with a particular disease, whereby the identification of specific biomarkers in the early stage of disease, improves the success of the therapy. However, a single value is not expressive for interpretation. Only the time progression of the biomarkers is interpretable. Due to its stability and its frequent existence in the human blood, it might be that GAD 65 could be a suitable candidate as biomarker for diabetes mellitus type 1. The results from the GAD 65 studies could also be important for the therapy of diabetes mellitus type 1 by passive administration of GAD 65 antibodies or even the application of GAD 65 for vaccination. First trials of injections with the antigen GAD 65 has been shown to preserve some insulin production for 30 months in humans with diabetes mellitus type 1. To gain more insight into the role of GAD 65 for early diagnosis and therapy, an additional screening of further samples, with corresponding case history, is planned. To use GAD 65 as a biomarker of diabetes mellitus type 1, a big longitudinal study will be necessary to follow children of high risk category by monitoring their GAD 65 serum level over time. By comparing to normal healthy subjects, a potential differentiator may be identified.

Author details

Wiltgen Marco* and Gernot P. Tilz
*Institute for Medical Informatics, Statistics and Documentation,
Medical University of Graz, Graz, Austria*

7. References

- [1] Tierney LM, S J McPhee SJ, Papadakis MA (2002) Current medical Diagnosis & Treatment. International edition. New York: Lange Medical Books/McGraw-Hill.
- [2] Rother KI (2007) Diabetes treatment—bridging the divide . The New England Journal of Medicine. 356(15): 1499–1501.
- [3] Duckworth WC, Kitabchi AE (1981) Insulin metabolism and degradation. Endocr Rev. 2:210–233.

* Corresponding Author

- [4] Duckworth WC (1988) Insulin degradation: mechanisms, products, and significance. *Endocr Rev.* 9:319–345.
- [5] Capes SE, Hunt D, Malmberg K, Pathak P, Gerstein HC (2001) Stress hyperglycemia and prognosis of stroke in nondiabetic and diabetic patients: a systematic overview. *Stroke.* 32(10): 2426–2432.
- [6] Hill NR, Thompson B, Bruce J, Matthews DR, Hindmarsh P (2009) Glycaemic risk assessment in children and young people with Type 1 diabetes mellitus. *Diabet Med.* 26(7):740-743.
- [7] Huysman E, Mathieu C (2009) Diabetes and peripheral vascular disease. *Acta Chir Belg.* 109(5):587-594.
- [8] Goyal BR, Solanki N, Goyal RK, Mehta AA (2009) Investigation into the cardiac effects of spironolactone in the experimental model of type 1 diabetes. *J Cardiovasc Pharmacol.* 54(6):502-509.
- [9] Vergès B (2009) Lipid disorders in type 1 diabetes. *Diabetes Metab.* 35(5):353-560.
- [10] Grauslund J, Hodgson L, Kawasaki R, Green A, Sjølie AK, Wong TY (2009) Retinal vessel calibre and micro- and macrovascular complications in type 1 diabetes. *Diabetologia.* 52(10):2213-2217.
- [11] Wild S, Roglic G, Green A, Sicree R, King H (2004) Global prevalence of diabetes: estimates for 2000 and projections for 2030. *Diabetes Care.* 27(5):1047–1053.
- [12] Craig ME, Hattersley A, Donaghue KC (2009) Definition, epidemiology and classification of diabetes in children and adolescents. *Pediatr Diabetes.* (10)12: 3-12.
- [13] Karagianni P, Sampanis Ch, Katsoulis Ch, Miserlis G, Polyzos S, Zografou I, Stergiopoulos S, Douloubakas I, Zamboulis Ch (2009) Continuous subcutaneous insulin infusion versus multiple daily injections. *Hippokratia.* 13(2):93-96.
- [14] Grossi SA, Lottenberg SA, Lottenberg AM, Della Manna T, Kuperman H (2009) Home blood glucose monitoring in type 1 diabetes mellitus. *Rev Lat Am Enfermagem.* 17(2):194-200.
- [15] Veleminsky Sr M, Buresova G (2008) Health Related Quality of Life of Children and Adolescents with Type 1 Diabetes. *Neuro Endocrinol Lett.* (5):29(6).
- [16] Report of the Expert Committee on the Diagnosis and Classification of Diabetes Mellitus. *Diabetes Care* 25, 2002.
- [17] Sabin MA, Cameron FJ, Werther GA (2009) Type 1 diabetes--still the commonest form of diabetes in children. *Aust Fam Physician.* 38(9):695-697.
- [18] Patterson CC, Dahlquist GG, Gyürüs E, Green A, Gyula Soltész G (2009) The EURODIAB study group: Incidence trends for childhood diabetes mellitus type 1 in Europe during 1989-2003 and predicted new cases 2005-2020: a multicentre prospective registration study. *The Lancet.* 373(9680):2027-2033.
- [19] Johnson JD, Luciani DS (2010) Mechanisms of Pancreatic beta-Cell Apoptosis in Diabetes and Its Therapies. *Adv Exp Med Biol.* 654:447-462.
- [20] Harrison LC (1992) Islet cell antigens in insulin-dependent diabetes: Pandora's box revisited. *Immunol Today.* 13(9):348-352.

- [21] Cooke DW, Plotnick L (2008) Type 1 diabetes mellitus in pediatrics. *Pediatr Rev.* 29(11):374–384.
- [22] Van der Werf N, Kroese FG, Rozing J, Hillebrands JL (2007) Viral infections as potential triggers of type 1 diabetes. *Diabetes Metab Res Rev.* 23(3):169-183.
- [23] Tirabassi RS, Guberski DL, Blankenhorn EP, Leif JH, Woda BA, Liu Z, Winans D, Greiner DL, Mordes JP (2010) Infection with viruses from several families triggers autoimmune diabetes in LEW*1WR1 rats: prevention of diabetes by maternal immunization. *Diabetes.* 59(1):110-118.
- [24] Richer MJ, Horwitz MS (2009) Preventing viral-induced type 1 diabetes. *Ann N Y Acad Sci.* 1173:487-492.
- [25] Burgess MA, Forrest JM (2009) Congenital rubella and diabetes mellitus. *Diabetologia.* 52(2):369-370.
- [26] Shehadeh N, Shamir R, Berant M, Etzioni A (2001) Insulin in human milk and the prevention of type 1 diabetes. *Pediatric Diabetes.* 2(4):175–177.
- [27] Virtanen SM, Knip M (2003) Nutritional risk predictors of beta cell autoimmunity and type 1 diabetes at a young age. *The American Journal of Clinical Nutrition.* 78(6):1053–1067.
- [28] Bantle JP (2009) Dietary fructose and metabolic syndrome and diabetes. *J Nutr.* 139(6):1263-1268.
- [29] Atkinson, M.A., Kaufman, D.L., Newman, D., Tobin, A.J. & Maclaren, N.K (1993) Islet cell cytoplasmic autoantibody reactivity to glutamate decarboxylase in insulin-dependent diabetes. *J. Clin. Invest.* 91:350–356.
- [30] Franke B, Galloway TS, Wilkin TJ (2005) Developments in the prediction of type 1 diabetes mellitus, with special reference to insulin autoantibodies. *Diabetes Metab Res Rev.* 21(5):395-415.
- [31] Tuomilehto J, Zimmet P, Mackay IR, Koskela P, Vidgren G, Toivanen L, Tuomilehto-Wolf E, Kohtamäki K, Stengård J, Rowley MJ (1994) Antibodies to glutamic acid decarboxylase as predictors of insulin-dependent diabetes mellitus before clinical onset of disease. *Lancet.* 343(8910):1383-1385.
- [32] Solimena, M. et al (1988) Autoantibodies to glutamic acid decarboxylase in a patient with stiff-man syndrome, epilepsy and type-1 diabetes. *N. Engl. J. Med.* 318: 1012–1020.
- [33] Solimena, M., Folli, F., Aparisi, R., Pozza, G. & De Camilli, P (1990) Autoantibodies to GABA-ergic neurons and pancreatic beta cells in stiff-man syndrome. *N. Engl. J. Med.* 322:1555–1560.
- [34] Baekkeskov, S. et al (1982) Autoantibodies in newly diagnosed diabetic children with immunoprecipitate human pancreatic islet cell proteins. *Nature.* 298: 167–169.
- [35] Jun HS, Khil LY, Yoon JW (2002) Role of glutamic acid decarboxylase in the pathogenesis of type 1 diabetes. *Cell Mol Life Sci.* 59:1892-1901.
- [36] Tilz GP, Dausset J, Wiltgen M (2009) The Diabetic Antigen Glutamic Acid Decarboxylase (GAD 65) in the Human Peripheral Blood. *Int Arch Allergy Immunol.* 16;152(2):184-194.

- [37] Tilz GP, Wiltgen M, Borkenstein M (2011) On the occurrence of the diabetes-associated antigen GAD 65 in human sera. *Int Arch Allergy Immunol.* 155(2):167-179.
- [38] Magde D, Elson EL, Webb WW (1974) Fluorescence correlation spectroscopy. II. An experimental realization. *Biopolymers.* 13(1):29-61.
- [39] Eigen M, Rigler R (1994) Sorting single molecules: application to diagnostics and evolutionary biotechnology. *Proc Natl Acad Sci USA.* 91:5740-5747.
- [40] Dittrich P, Malvezzi-Campeggi F, Jahnz M, Schwille P (2001) Accessing molecular dynamics in cells by fluorescence correlation spectroscopy. *Biol Chem.* 382(3):491-494.
- [41] Schwille P (2001) Fluorescence correlation spectroscopy and its potential for intracellular applications. *Cell Biochem Biophys.* 34(3):383-408.
- [42] Medina MA, Schwille P (2002) Fluorescence correlation spectroscopy for the detection and study of single molecules in biology. *Bioessays.* 24(8):758-764.
- [43] Schlaman HR, Schmidt K, Ottenhof D, van Es MH, Oosterkamp TH, Spaank HP (2008) Analysis of interactions of signaling proteins with phage-displayed ligands by fluorescence correlation spectroscopy. *J Biomol Screen.* 13(8):766-776.
- [44] Van Weemen BK, Schuurs AH (1971) Immunoassay using antigen-enzyme conjugates. *FEBS Letters.* 15(3):232-236.
- [45] Engvall E, Perlman P (1971) Enzyme-linked immunosorbent assay (ELISA). Quantitative assay of immunoglobulin G. *Immunochemistry.* 8(9): 871-874.
- [46] S. Leng, J. McElhaney, J. Walston, D. Xie, N. Fedarko, G. Kuchel (2008) Elisa and Multiplex Technologies for Cytokine Measurement in Inflammation and Aging Research. *J Gerontol A Biol Sci Med Sci.* 63:879-884.
- [47] Bexley J, Hogg JE, Hammerberg B, Halliwell RE (2009) Levels of house dust mite-specific serum immunoglobulin E (IgE) in different cat populations using a monoclonal based anti-IgE enzyme-linked immunosorbent assay. *Vet Dermatol.* 20(5-6): 562-568.
- [48] Nishifuji K, Tamura K, Konno H, Olivry T, Amagai M, Iwasaki T (2009) Development of an enzyme-linked immunosorbent assay for detection of circulating IgG autoantibodies against canine desmoglein 3 in dogs with pemphigus. *Vet Dermatol.* 20(5-6):331-337.
- [49] Thomson G (1956) Centenary of J. J. Thomson. *Science.* 124(3233):1191-1195.
- [50] Koomen J, Hawke D, Kobayashi R (2005) Developing an understanding of proteomics: an introduction to biological mass spectrometry. *Cancer Invest.* 23(1):47-59.
- [51] Dijkstra M, Vonk RJ, Jansen RC (2007) SELDI-TOF mass spectra: A view on sources of variation. *Journal of Chromatography B.* (847): 12-23.
- [52] Issaq HJ, Conrads TP, Prieto DA, Tirumalai R, Veenstra TD (2003) SELDI-TOF MS for diagnostic proteomics. *Analytical Chemistry A.* 149-155.
- [53] Clarke CH, Buckley JA, Fung ET (2005) SELDI-TOF-MS proteomics of breast cancer. *Clin Chem Lab Med.* 43,12:1314-1320.
- [54] Boyce EA, Kohn EC (2005) Ovarian cancer in the proteomics era: diagnosis, prognosis and therapeutics targets. *Int J Gynecol cancer.* 15: 266-373.

- [55] Vorderwülbecke S, Cleverley S, Weinberger SR, Wiesner A (2005) Protein quantification by the SELDI-TOF-MS-based ProteinChip System. *Nature Methods*. 2,5:393-395.
- [56] Gast MC, Van Gils CH, Wessels LF, Harris N, Bonfrer JM, Rutgers EJ, Schellens JH, Beijnen JH (2009) Serum protein profiling for diagnosis of breast cancer using SELDI-TOF. *MS.Oncol Rep*. 22(1):205-213.
- [57] Myers MA, Fenalti G, Gray R, Scealty M, Tong JC, El-Kabbani O, Rowley MJ (2003) A diabetes-related epitope of GAD65: a major diabetes-related conformational epitope on GAD65. *Ann NY Acad Sci*. 1005: 250-252.
- [58] Schwartz HL, Chandonia JM, Kash SF, Kanaani J, Tunnell E, Domingo A, Cohen FE, Banga JP, Madec AM, Richter W, Baekkeskov S (1999) High-resolution autoreactive epitope mapping and structural modelling of the 65 kDa form of glutamic acid Decarboxylase. *J Mol Biol*. 287: 983-999.
- [59] Fenalti G, Law RH, Buckle AM, Langendorf C, Tuck Rosado CJ, Faux NG, Mahmood K, Hampe CS, Banga JP, Wilce M, Schmidberger J, Rossjohn J, El-Kabbani O, Pike RN, Smith AI, Mackay IR, Rowley MJ, Whisstock JC (2007) GABA production by glutamic acid decarboxylase is regulated by a dynamic catalytic loop. *Struct. Mol. Biol*. 14, 280-286.
- [60] Guex N, Peitsch MC (1997) SWISS-MODEL and the Swiss-Pdb Viewer: An environment for comparative protein modelling. *Electrophoresis*. 18:2714-2723.
- [61] Berman HM, Westbrook J, Feng Z, Gilliland G, Bhat TN, Weissig H, Shindyalov IN, Bourne PE (2000) The PDB data uniformity project. *Nucleic Acids Research*. 28:235-242.
- [62] Edelsbrunner H, Harer JL (2010) *Computational Topology. An Introduction*. Amer. Math. Soc., Providence, Rhode Island.
- [63] Liang J, Edelsbrunner H, Woodward C (1998) Anatomy of protein pockets and cavities: measurement of binding site geometry and implications for ligand design. *Protein Science*. 7:1884-1897.
- [64] Edelsbrunner H, Facello MA, Liang J (1998) On the definition and the construction of pockets in macromolecules. *Discrete Appl. Math*. 88:83-102.
- [65] Headd J., Ban YHA, Brown P, Edelsbrunner H, Vaidya M, Rudolph J (2007) Protein-protein interfaces: properties, preferences, and projections. *Proteome Research*. 6:2576-2586.
- [66] Voronoi G (1908) Recherche sur les paralleloedres primitifs. *J. Reine Angw Math* 134:198-287.
- [67] Dupuis F, Sadoc JF, Mornon JP (2004) Protein Secondary Structure Assignment Through Voronoi Tessellation. *Proteins: Structure, Function, and Bioinformatics*. 55:519-528.
- [68] Angelov B, Sadoc JF, Jullien R, Soyer A, Mornon JP, Chomilier J (2002) Nonatomic Solvent-Driven Voronoi Tessellation of Proteins: A Open Tool to Analyze Protein Folds. *Proteins: Structure, Function, and Genetics*. 49:446-456.
- [69] Dupuis F, Sadoc JF, Jullien R, Angelov B, Mornon J (2005) Voro3D: 3D voronoi tessellations applied to protein structures. *Bioinformatics*. 21(8):1715-1716.

- [70] Perruccio F, Ridder L, Mulholland AJ (2003) Quantum-mechanical/Molecular-mechanical Methods in Medicinal Chemistry, In: Carloni P, Alber F (Eds), Quantum Medicinal Chemistry. WILEY_VCH Verlag GmbH&Co. Weinheim.
- [71] Jensen F (2007) Introduction to computational chemistry. John Wiley&Sons Ltd, UK.
- [72] Szabo A, Ostlund NS (1996) Modern quantum chemistry. Dover Publications, INC, Mineola, New York.
- [73] Corper AL, Stratmann T, Apostolopoulos V, Scott CA, Garcia KC, Kang AS, Wilson IA, Teyton L (2000) A structural framework for deciphering the link between I-Ag7 and autoimmune diabetes. *Science*. 21;288(5465):505-511.